nature communications

Article

https://doi.org/10.1038/s41467-025-67044-5

Biguanide-functionalized peptide mimics effectively combat drug-resistant ESKAPE pathogens and meningitis

Received: 16 March 2025

Accepted: 20 November 2025

Published online: 09 December 2025

Check for updates

Weinan Jiang[1], Min Zhou[2], Kang Chen[2], Ximian Xiao[2], Jia Shi[2], Haodong Zhang[2], Jiayang Xie[1], Sheng Chen[2], Minzhang Chen[2], Zihao Cong[2], Longqiang Liu[2], Yueming Wu[2,3,4,5,6,7] & Runhui Liu[1,2,3,4,5,6,7,8]

ESKAPE pathogens-induced meningitis seriously threatens human health due to antimicrobial resistance and low permeability of blood-brain barrier (BBB). It's a promising strategy to combat drug-resistant pathogens using synthetic mimics of host defense peptide (HDP) bearing positive charges that are mainly provided by amine or guanidine. Here, we report that biguanide serves as a type of positively charged moiety to design HDP mimics. Biguanide exerts a stronger interaction with bacterial membrane phospholipids via bidentate hydrogen bonds than do amine and guanidine. The biguanide-functionalized HDP mimic, $PBGProOx_{20}$, targets bacterial membrane phospholipids to show potent activity against all ESKAPE pathogens and does not induce antimicrobial resistance. $PBGProOx_{20}$ exhibits promising BBB-penetrating property and displays potent therapeutic effects in female mice full-thickness infection model, sub-cutaneous infection model, kidney infection model, peritonitis model, and meningitis model. This study provides a promising strategy for designing HDP mimics to combat ESKAPE pathogens and meningitis.

Bacterial meningitis poses a serious threat to human health with a mortality rate reaching up to 54%[1], particularly when caused by multidrug-resistant ESKAPE pathogens, including *Enterococcus faecium*, *Staphylococcus aureus*, *Klebsiella pneumoniae*, *Acinetobacter baumannii*, *Pseudomonas aeruginosa*, and *Enterobacter* species[2,3]. The blood-brain barrier (BBB) further limits the clinical selection and efficacy of antibiotics[4]. Thus, it is urgent to develop potent antimicrobials with broad-spectrum activity and BBB penetrating property for the treatment of ESKAPE pathogens-induced infections, especially meningitis. Host defense peptides (HDPs) have been widely studied as potential anti-infective alternatives of antibiotics owing to their broad-spectrum antimicrobial activity and low tendency to induce antimicrobial resistance[5–9]. However, inherent limitations of HDPs such as low protease stability, high cost, and cumbersome synthesis have

[1]Suzhou Institute of Biomedical Engineering and Technology, Chinese Academy of Sciences, Suzhou, China. [2]State Key Laboratory of Bioreactor Engineering, East China University of Science and Technology, Shanghai, China. [3]Shanghai Frontiers Science Center of Optogenetic Techniques for Cell Metabolism, School of Materials Science and Engineering, East China University of Science and Technology, Shanghai, China. [4]Frontiers Science Center for Materiobiology and Dynamic Chemistry, School of Materials Science and Engineering, East China University of Science and Technology, Shanghai, China. [5]Engineering Research Center for Biomedical Materials of Ministry of Education, School of Materials Science and Engineering, East China University of Science and Technology, Shanghai, China. [6]Key Laboratory for Ultrafine Materials of Ministry of Education, School of Materials Science and Engineering, East China University of Science and Technology, Shanghai, China. [7]Key Laboratory of Specially Functional Polymeric Materials and Related Technology (Ministry of Education), School of Materials Science and Engineering, East China University of Science and Technology, Shanghai, China. [8]Shanghai Shyndec Pharmaceutical Co., Ltd., Shanghai, China. e-mail: yuemingwu@ecust.edu.cn; rliu@ecust.edu.cn

restricted their applications[10]. Consequently, HDPs mimics are actively studied, aiming to address drug-resistant bacterial infections[11–22]. However, currently there are few reports displaying therapeutic efficacy in bacterial meningitis[23].

Cationic HDPs and their mimics exert antimicrobial activity through initial interactions with the negatively charged phospholipids of bacteria, primarily using amine or guanidine moieties as cationic groups (Fig. 1a)[24–37]. However, achieving dual-functional HDP mimics with potent anti-ESKAPE activity and BBB-penetrating ability using these two moieties remains challenging[38–44]. We turn attention to an alternative positively charged moiety, biguanide, which possesses higher positive charge density than amine and guanidine, as revealed by density functional theory calculations (Fig. 1b). The planar, conjugated cationic structures of biguanide enable simultaneous donation of two hydrogen bonds to anionic phosphate headgroups of bacterial membrane phospholipids (Fig. 1c). This dual-point attachment generates cooperative electrostatic interaction and bidentate hydrogen bonds, significantly enhancing membrane binding affinity and

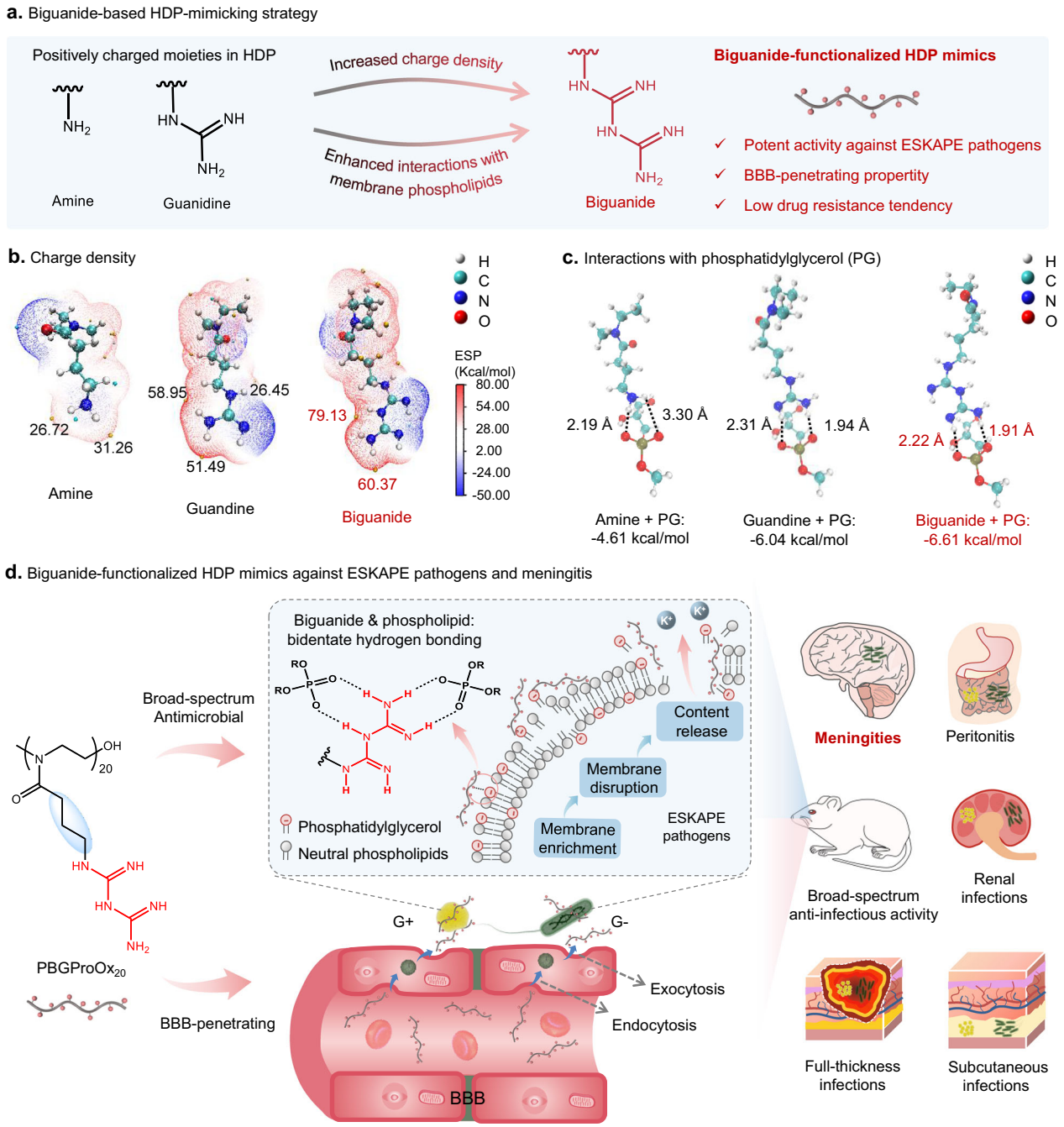

Fig. 1 | Design of biguanide-functionalized HDP mimics. a The proposed antimicrobial design strategy that biguanide serves as a type of positively charged moiety to design host defense peptides (HDPs) mimics. **b** The restrained electrostatic potential (ESP) energy surface of different positively charged moieties (amine, guanidine, and biguanide). Significant surface local minima and maxima of ESP are represented as orange and cyan spheres. **c** Snapshots of conformations between negatively charged phosphatidylglycerol and different positively charged groups (amine, guanidine, and biguanide) at the positions where the free energy reaches a minimum. Biguanide showed a more favorable alignment and hydrogen bonding with phosphatidylglycerol than amine or guanidine. **d** The biguanide-functionalized poly(2-oxazoline) possesses broad-spectrum antimicrobial activity and blood-brain barrier (BBB) penetrating property, thus showing potent therapeutic efficacy in multiple infection models, including meningitis.

disruption efficiency[45]. The higher localized positive charge density also endows biguanide-based compounds more efficient initial electrostatic interaction with negatively charged luminal surface of BBB, thereby potentially enhancing its BBB penetration efficiency via adsorptive-mediated transcytosis, which is a crucial pathway for positively charged molecules to enter the brain[46,47]. Thus, we hypothesize that biguanide can serve as a type of positively charged moiety for HDP mimics to exert broad-spectrum activity and BBB-penetrating property to combat drug-resistant infections caused by ESKAPE pathogens, especially meningitis (Fig. 1a).

In this study, we explore biguanide-functionalized HDP mimics using poly(2-oxazoline)s as the backbone structure that was recently reported to be a peptide-mimicking scaffold by our group[48–51]. The optimal compound, PBGProOx$_{20}$, demonstrates broad-spectrum activities against multi-drug resistant bacteria and mature biofilms, including all ESKAPE pathogens, via a membrane-disrupting mechanism (Fig. 1d). Notably, the repeated use of PBGProOx$_{20}$ doesn't induce bacteria to develop resistance against PBGProOx$_{20}$ and cross-resistance against commonly used antibiotics. PBGProOx$_{20}$ displays potent therapeutic efficacy against ESKAPE pathogens in multiple models of drug-resistant bacterial infections in mice, including full-thickness wound infections, subcutaneous infections, kidney infections, and peritonitis (Fig. 1d). Moreover, PBGProOx$_{20}$ effectively penetrates BBB through transcytosis across brain endothelial cells and exerts promising therapeutic effects in treating bacterial meningitis. Our findings suggest that biguanide-functionalized HDP mimics represent a promising strategy to develop antimicrobials with potent activities against all ESKAPE pathogens and BBB penetration to treat bacterial meningitis.

Results

Synthesis of biguanide-functionalized poly(2-oxazoline)s with variable spacer groups

A series of HDP-mimicking poly(2-oxazoline)s were synthesized with positively charged biguanide groups and variable sidechain spacer groups. Briefly, amine-functionalized poly(2-oxazoline)s were synthesized through methyl trifluoromethanesulfonate (MeOTf)-initiated polymerization of 2-oxazolines featuring diverse side chains, followed by trifluoroacetic acid (TFA) treatment to remove the *N*-Boc protecting groups (Fig. 2a, and Supplementary Figs. 1-15). The obtained amine-functionalized poly(2-oxazoline)s were treated with *N*-Amidinopyrazole-1-carboxamidine to afford the biguanide-functionalized poly(2-oxazoline)s in a single step (Supplementary Figs. 16-19)[52]. The resulting poly(2-oxazoline)s, featuring biguanide groups and variable sidechain spacer groups (methan−, ethan−, propan−, butan−, pentan−), were obtained at around 20 mer (DP = 20) at a narrow dispersity (1.07–1.26), according to the characterization using gel permeation chromatography (GPC) (Fig. 2b, Supplementary Fig. 20, Table S1). The successful functionalization of poly(2-oxazoline)s with biguanide groups was confirmed by ^{1}H NMR spectra (Supplementary Figs. 21–30). The strong electron-withdrawing effect and high charge density of the biguanide moiety induced a notable downfield shift of the proton peak from 'H_N' (δ-3.0 ppm for −C$\underline{H_2}$−amine) to 'H_B' (δ-3.2 ppm for −C$\underline{H_2}$−biguanide), with no residual upfield peaks attributable to unconverted amine groups observed, indicating virtually complete functionalization (Fig. 2c).

As described above, the synthetic process of biguanide-functionalized poly(2-oxazoline)s can be completed in as fast as 12 h. In contrast, solid-phase-peptide synthesis (SPPS) is the most common method for HDPs synthesis[53]. The sequential grafting of amino acids and repeated deprotection steps, along with complex purification schemes, significantly increase synthetic difficulty, period and limit quantities of the final product. Solid-phase synthesis of HDPs often continuously consumes excess expensive coupling reagents and protected amino acids. In contrast, the fast synthesis and cheap reactants make poly(2-oxazoline)s significantly more cost-effective and accessible, overcoming key limitations of HDPs such as high cost and difficult synthesis.

In vitro antimicrobial activity and toxicity of biguanide-functionalized poly(2-oxazoline)s

The antimicrobial efficacy of the biguanide-functionalized poly(2-oxazoline)s with various sidechain spacers against six ESKAPE pathogens was quantified using the minimum inhibitory concentrations (MIC). These polymers exhibited potent activity against gram-positive bacteria (*S. aureus* and *E. faecium*), with MICs ranging between 6.25 and 12.5 μg/mL (Fig. 2d). Notably, the biguanide-functionalized poly(2-oxazoline) bearing a propane side-chain spacer, PBGProOx$_{20}$, outperformed other polymers against gram-negative bacteria, including *K. pneumoniae*, *A. baumannii*, *P. aeruginosa*, and *E. coli*, with MICs ranging from 6.25 to 25 μg/mL. Moreover, these polymers displayed negligible hemolysis against red blood cells and cytotoxicity toward COS7 kidney cells, with HC_{10} and IC_{50} values exceeding 2000 μg/mL and 400 μg/mL, respectively (Fig. 2e). The antimicrobial selectivity index (SI) of these polymers was calculated from HC_{10}/MIC and IC_{50}/MIC, respectively. Among these polymers, PBGProOx$_{20}$ demonstrated superior antimicrobial selectivity against all drug-resistant ESKAPE pathogens, with SI surpassing 80 (HC_{10}/MIC) and 32 (IC_{50}/MIC) (Tables S2 and S3).

Poly(hexamethylene biguanide) (PHMB) is a broad-spectrum antimicrobial agent and is approved as a disinfectant used for topical wound care. However, the antimicrobial activity of PHMB is primarily attributed to the dense linear arrangement of biguanide groups, resulting in potential toxicity that limits its in vivo applications. The HDP-mimicking poly(2-oxazoline)s deliberately incorporate biguanide moieties sparsely and controllably onto the highly tunable, flexible, and biocompatible poly(2-oxazoline) backbone. The poly(2-oxazoline) was recently reported to be a peptide-mimicking scaffold by our group[50,51], which provides a modular platform to fine-tune the hydrophobic/hydrophilic balance, chain length, and biguanide spacing, enabling the optimization of antimicrobial activity and toxicity. We also compared the antimicrobial activity, hemolysis, cytotoxicity and antimicrobial selectivity of PHMB (Table S4). While PHMB showed potent antimicrobial efficacy (MIC = 0.39 - 6.25 μg/mL), substantial hemolysis and cytotoxicity (HC_{10} = 3.13 μg/mL, IC_{50} = 25 μg/mL) greatly weakened its antimicrobial selectivity. PBGProOx$_{20}$ demonstrates significantly better antimicrobial selectivity against ESKAPE pathogens and has greater potential for treating drug-resistant bacterial infections.

To further elucidate the impact of polymer chain length on antimicrobial performance, we synthesized biguanide-functionalized poly(2-oxazoline)s (PBGProOx$_n$) bearing a propane sidechain spacer and variable chain lengths (5, 10, 20, and 40 mer) at a narrow dispersity (1.10–1.23) (Supplementary Fig. 31, and Table S5). Among these polymers, PBGProOx$_{20}$ and PBGProOx$_{40}$ demonstrated potent antimicrobial efficacy against all six ESKAPE pathogens with MICs in the range of 6.25 to 25 μg/mL, superior to 5 and 10 mer polymers (Fig. 2f). Moreover, PBGProOx$_{20}$ exhibited lower cytotoxicity (IC_{50} > 400 μg/mL) than PBGProOx$_{40}$ (Fig. 2g). We also evaluated the cytotoxicity of PBGProOx$_{20}$ on primary cells and found that bone marrow mesenchymal stromal cells (BMSCs) retained ~100% viability even after 24-h treatment with 400 μg/mL of PBGProOx$_{20}$ (Supplementary Fig. 32). Collectively, these results suggest PBGProOx$_{20}$ as the optimal antimicrobial polymer for further study.

The broad-spectrum antimicrobial activities of PBGProOx$_{20}$ were further assessed against multiple clinically isolated bacterial strains, comprising 13 gram-positive strains and 17 gram-negative strains. Most of these pathogens were drug-resistant or even multidrug-resistant to tested antibiotics, including ampicillin, vancomycin, streptomycin, imipenem, and norfloxacin (Fig. 2h, i, and Tables S6 and S7). In sharp contrast, PBGProOx$_{20}$ was active against all these drug-resistant

https://doi.org/10.1038/s41467-025-67044-5

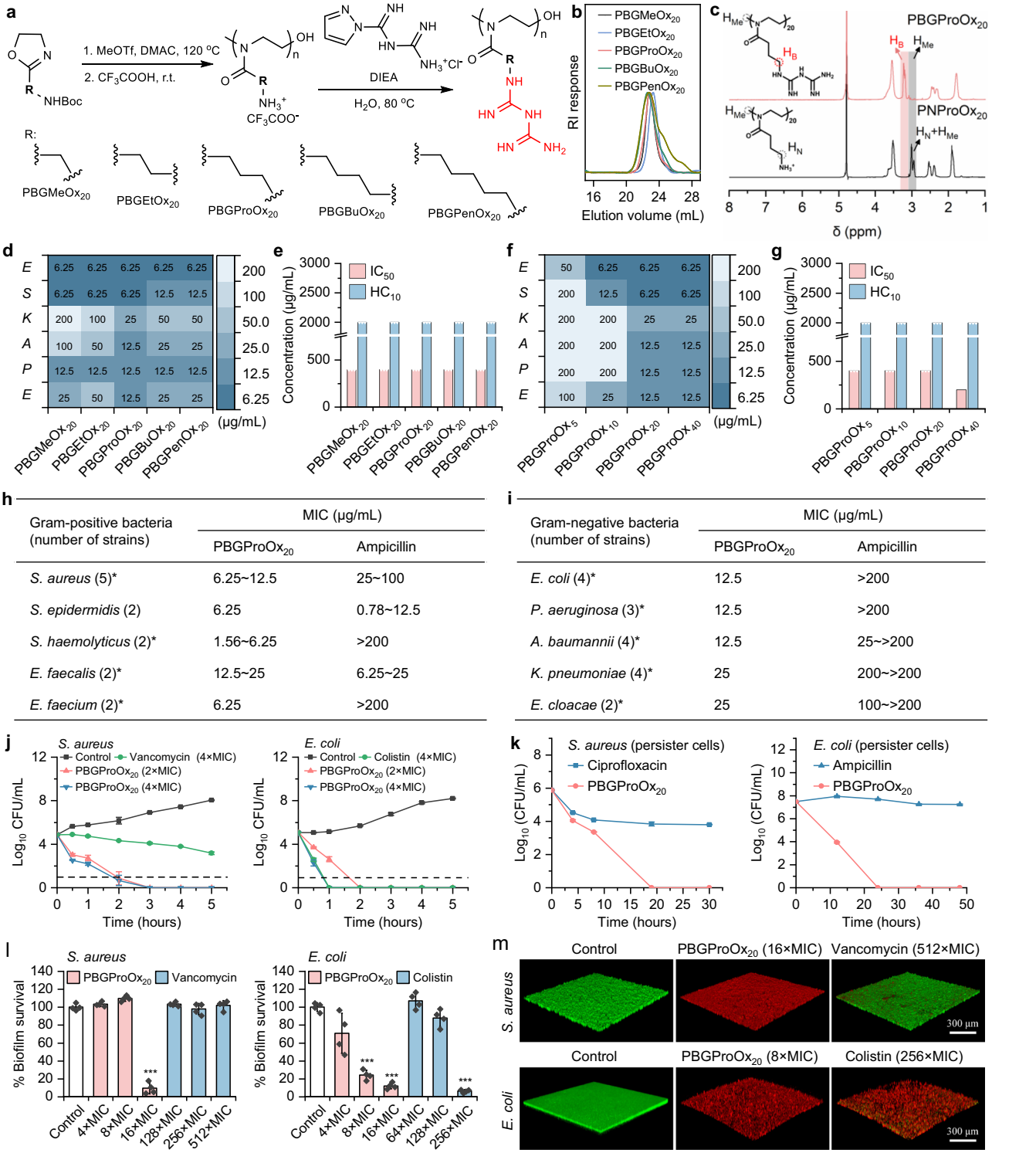

Gram-positive bacteria (number of strains)	MIC (μg/mL)	
	$PBGProOx_{20}$	Ampicillin
S. aureus (5)*	6.25~12.5	25~100
S. epidermidis (2)	6.25	0.78~12.5
S. haemolyticus (2)*	1.56~6.25	>200
E. faecalis (2)*	12.5~25	6.25~25
E. faecium (2)*	6.25	>200

Gram-negative bacteria (number of strains)	MIC (μg/mL)	
	$PBGProOx_{20}$	Ampicillin
E. coli (4)*	12.5	>200
P. aeruginosa (3)*	12.5	>200
A. baumannii (4)*	12.5	25~>200
K. pneumoniae (4)*	25	200~>200
E. cloacae (2)*	25	100~>200

bacteria, with MIC values ranging from 1.56 to 25 μg/mL against gram-positive bacteria and from 12.5 to 25 μg/mL against gram-negative bacteria (Fig. 2h, i).

To evaluate $PBGProOx_{20}$'s proteolytic stability, trypsin was used as a representative enzyme for enzymatic degradation studies. Following trypsin treatment, $PBGProOx_{20}$ retained its broad-spectrum antimicrobial activity against *S. aureus* and *E. coli* (Supplementary Fig. 33). This contrasts sharply with the classical HDP melittin, which completely lost its antimicrobial activity (MIC increased from 6.25 μg/mL to >200 μg/mL). Furthermore, NMR analysis showed no structural changes in $PBGProOx_{20}$ after 7 days exposure to trypsin (Supplementary Fig. 34). These results demonstrate the poly(2-oxazoline)'s significantly greater resistance to enzymatic degradation compared to HDPs.

In vitro broad-spectrum antimicrobial performance of $PBGProOx_{20}$

We further studied the time-killing kinetics of $PBGProOx_{20}$ against *S. aureus* and *E. coli* in the exponential growth phase. It was found that $PBGProOx_{20}$ at a concentration of 2×MIC and 4×MIC completely eradicated *S. aureus* and *E. coli* within three or two hours, respectively (Fig. 2j). $PBGProOx_{20}$ exhibited rapid killing efficacy comparable to

Fig. 2 | Synthesis and in vitro broad-spectrum antimicrobial performance of biguanide-functionalized poly(2-oxazoline)s. a Synthesis of biguanide-functionalized poly(2-oxazoline)s with various side-chain spacers and chain lengths. **b** GPC traces of poly(2-oxazoline)s with various side-chain spacers. **c** ^{1}H NMR characterization of biguanide-functionalized poly(2-oxazoline) $PBGProOx_{20}$ and amine-functionalized poly(2-oxazoline) $PNProOx_{20}$. **d** Antimicrobial activity of biguanide-functionalized poly(2-oxazoline)s against ESKAPE pathogens, including *E. faecium* (*E*), *S. aureus* (*S*), *K. pneumoniae* (*K*), *A. baumannii* (*A*), *P. aeruginosa* (*P*), *E. coli* (*E*). All these bacteria are drug resistant or multi-drug resistant strains. **e** Hemolysis and cytotoxicity of biguanide-functionalized poly(2-oxazoline)s with various side-chain spacers. **f** Antimicrobial activity of biguanide-functionalized poly(2-oxazoline)s $PBGProOx_n$ with different chain lengths against ESKAPE pathogens. **g** Hemolysis and cytotoxicity of biguanide-functionalized poly(2-oxazoline)s $PBGProOx_n$ with different chain lengths. Antimicrobial activity of $PBGProOx_{20}$ and ampicillin against clinically isolated gram-positive bacteria (**h**) and gram-negative bacteria (**i**). *All these bacteria are clinically isolated drug-resistant pathogens. **j** Time killing kinetics of $PBGProOx_{20}$ (2×MIC, 4×MIC) against *S. aureus* and *E. coli* at exponential growth phase, using vancomycin (4×MIC) and colistin (4×MIC) as the antibiotic controls, respectively ($n = 3$). The detection limit for viable bacterial concentration is 10 CFU/mL, as indicated by the dashed line. Data points below this threshold are designated as 0 CFU/mL. **k** Time killing kinetics of $PBGProOx_{20}$ (4×MIC) against persister cells of *S. aureus* and *E. coli* ($n = 3$). Ciprofloxacin (10×MIC) or ampicillin (8×MIC) treatment were used as the control. **l** The ability of $PBGProOx_{20}$ and antibiotics at different concentrations to eradicate mature biofilms of *S. aureus* and *E. coli* ($n = 4$). Statistical analysis between the two groups was performed using two-tailed *t*-test. $^{***}P < 0.001$. Exact *p* values are provided in Source Data. **m** Live-dead staining confocal images of mature biofilms after treatment with $PBGProOx_{20}$ and antibiotics. Data are presented as mean ± SD in **j**–**l**.

that of colistin against *E. coli*; whereas, vancomycin at a concentration of 4×MIC was unable to eradicate *S. aureus* after 5-h treatment. Compared with exponential-phase bacteria, persister cells pose a significant challenge due to their dormant state and increased resistance to antibiotics, frequently leading to recurrent infections post-therapy[54]. Notably, $PBGProOx_{20}$ eliminated persister cells within 24 h at a concentration of 4×MIC, achieving a reduction exceeding 6 logs in colony-forming units (CFU) (Fig. 2k). In sharp contrast, persister cells of *S. aureus* and *E. coli* still maintained sustained viability even after treatment with high-dose ciprofloxacin or ampicillin.

The established biofilms, predominantly composed of dormant bacterial persister cells, render conventional antibiotics largely ineffective[55]. The efficacy of $PBGProOx_{20}$ in eradicating mature biofilms was evaluated and compared with vancomycin and colistin, two critical last-resort antibiotics. Vancomycin demonstrated poor anti-biofilm activity against *S. aureus* biofilm even at a high concentration of 512×MIC (Fig. 2l). Similarly, colistin exhibited effectiveness against *E. coli* biofilm only at a high concentration of 256×MIC, underscoring the robust tolerance of biofilms to antibiotic treatments (Fig. 2l). In contrast, $PBGProOx_{20}$ effectively eradicated mature biofilms of *S. aureus* and *E. coli* at remarkably lower concentrations of 16×MIC and 8×MIC, respectively. Confocal microscopy images of live/dead-stained biofilms unequivocally demonstrated the capability of $PBGProOx_{20}$ to effectively eliminate bacterial persister cells within biofilms (Fig. 2m). Consequently, $PBGProOx_{20}$ exhibited broad-spectrum and potent antimicrobial activities superior to conventional antibiotics, particularly in targeting persister cells and mature biofilms.

Antimicrobial mechanism of $PBGProOx_{20}$

The superior antimicrobial performance of $PBGProOx_{20}$ against drug-resistant bacteria motivated us to investigate the antimicrobial mechanism. The fluorescent dye (morpholino-naphthalimide) labeled polymer (dye-$PBGProOx_{20}$) with green fluorescence was synthesized via bromide-initiated polymerization on 2-oxazoline $ProNH_{Boc}Ox$, followed by *N*-Boc deprotection and biguanidylation steps (Supplementary Figs. 35a and 36a). Time-lapse fluorescence confocal imaging was employed to visualize the intracellular localization of dye-$PBGProOx_{20}$ within *S. aureus* and *E. coli*, using propidium iodide (PI, red fluorescence) as the indicator probe for cell death (Fig. 3a, b). The fluorescent images and intensity analysis revealed rapid accumulation of dye-$PBGProOx_{20}$ on the membrane of *S. aureus* and *E. coli* within 1 min (Fig. 3c, d). The fluorescence signals from both dye-$PBGProOx_{20}$ and PI were observed in the cytoplasm of *S. aureus* after around 11 min of incubation, indicating membrane damage and subsequent entry of dye-$PBGProOx_{20}$ and PI into the bacterial cells (Fig. 3c, e). In the case of *E. coli*, the fluorescence of dye-$PBGProOx_{20}$ was mainly observed on the cell membrane throughout our observation, despite PI had penetrated into the cytoplasm (Fig. 3d, e).

The $PBGProOx_{20}$-treated bacterial cells also showed membrane-associated discontinuous red fluorescence puncta after staining with the membrane dye FM4-64, indicating perturbations to membrane lipid structure (Fig. 3f). Additionally, SYTOX was used as a probe for membrane integrity to show that $PBGProOx_{20}$ treatment damaged bacterial membranes in a concentration-independent manner (Fig. 3g). Scan electron microscopy (SEM) was employed to characterize the morphology changes of bacterial membrane. It was found that $PBGProOx_{20}$ treatment caused obvious wrinkling and collapse of the membrane in both *S. aureus* and *E. coli* (Fig. 3h). Transmission electron microscope (TEM) further validated that $PBGProOx_{20}$ caused significant membrane breakage, leakage of intracellular contents, and formation of extensive internal voids (Fig. 3i).

To figure out the mode of action of $PBGProOx_{20}$ on bacterial cell membranes and how biguanide outperforms amine or guanidine, multiply studies were conducted to compare polymer-bacterial membrane interaction using poly(2-oxazolie)s with positively charged moieties, $PNProOx_{20}$, $PGProOx_{20}$ and $PBGProOx_{20}$ (Fig. 4a). In the octanol-water partition study, all three polymers, dye-$PNProOx_{20}$, dye-$PGProOx_{20}$, and dye-$PBGProOx_{20}$, partitioned almost exclusively into the water layer due to their charged nature in the absence of any additives (Supplementary Fig. 37). However, dye-$PBGProOx_{20}$ exhibited significant partitioning into the octanol phase at lower equivalents of sodium laurate surrogate (a membrane-bound fatty acid salt) than dye-$PNProOx_{20}$ and dye-$PGProOx_{20}$. As sodium laurate concentration increased, dye-$PBGProOx_{20}$ was almost entirely partitioned into the octanol layer. This finding demonstrated that $PBGProOx_{20}$ exhibited greater affinity for the membrane and more effectively translocated into the membrane-mimic lipophilic layer".

We then assessed the impact of these polymers on cytoplasmic membrane potential using $DiSC_3(5)$, and found that $PBGProOx_{20}$ induced more significant membrane depolarization in both *S. aureus* and *E. coli* at different concentrations compared to $PNProOx_{20}$ and $PGProOx_{20}$ (Fig. 4b). Moreover, the membrane zeta potential of both *S. aureus* and *E. coli* shifted from below −15 mV to above +5 mV after treatment with $PBGProOx_{20}$, even at a low concentration of 0.5×MIC (Fig. 4c). $PBGProOx_{20}$ induced larger membrane zeta potential shifts than $PNProOx_{20}$ and $PGProOx_{20}$, indicating its greater accumulation on bacterial membranes. We then detected membrane fluidity using Laurdan as a fluorescent probe (Fig. 4d). Compared to $PNProOx_{20}$ and $PGProOx_{20}$, $PBGProOx_{20}$ treatment induced a greater increase in Laurdan fluorescence, revealing a more pronounced reduction in membrane fluidity in both *S. aureus* and *E. coli*. The ΔpH of bacterial cells, a key component of the proton motive force, was also evaluated using the fluorescent probe BCECF-AM (Fig. 4e). A more marked dissipation of ΔpH was observed in both *S. aureus* and *E. coli* after treatment with $PBGProOx_{20}$. These findings demonstrate that biguanide-functionalized $PBGProOx_{20}$ accumulates more effectively in bacterial membranes, inducing membrane potential derangement and decreasing membrane rigidity. This disturbs bacterial homeostasis and leads to critical metabolic dysfunctions, notably the dissipation of the proton motive force[56,57].

https://doi.org/10.1038/s41467-025-67044-5

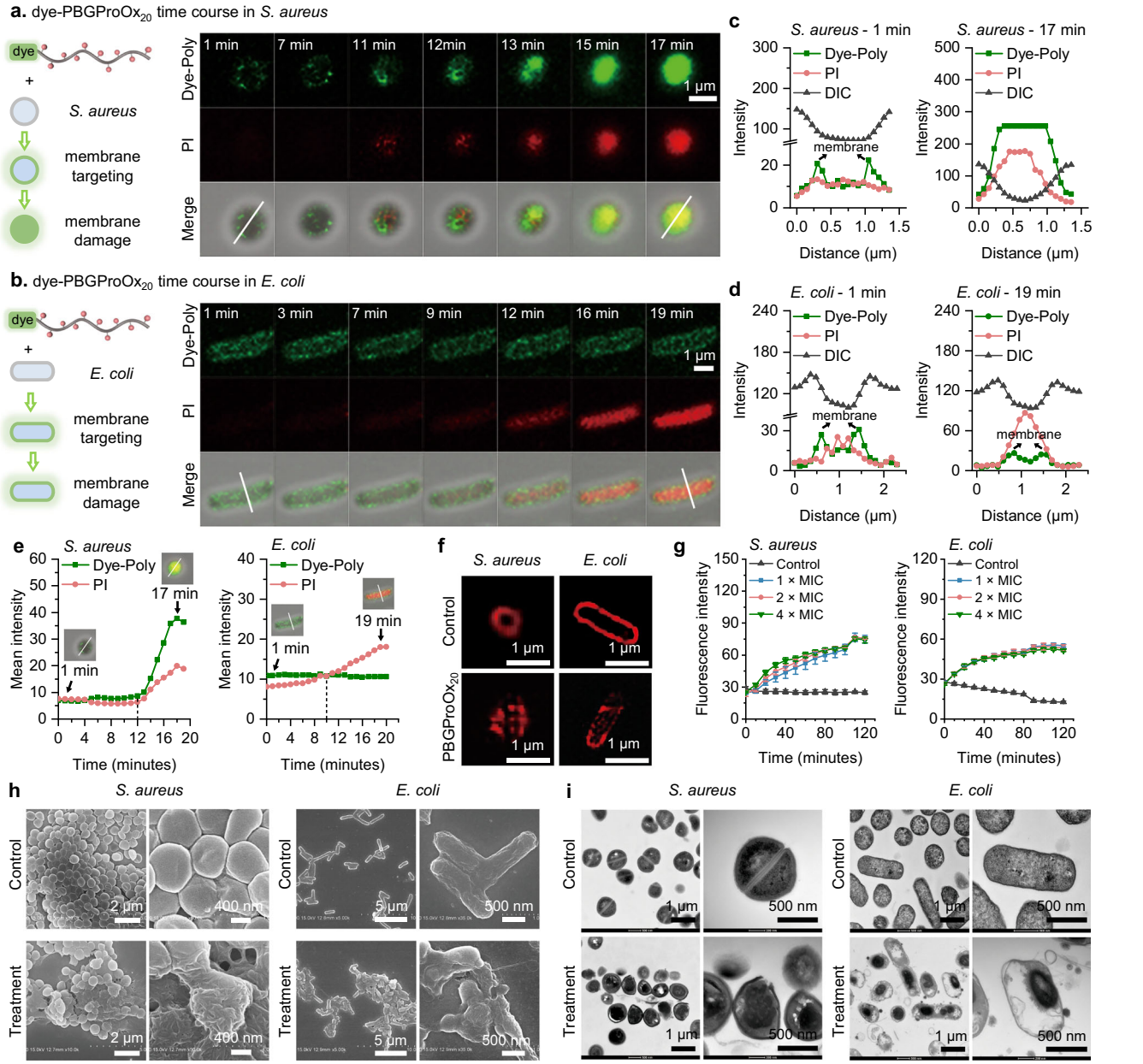

Fig. 3 | PBGProOx$_{20}$ exerts bactericidal activity by destroying bacterial membranes. Time-laps confocal images of *S. aureus* (**a**) and *E. coli* (**b**) at the presence of dye-PBGProOx$_{20}$ (green, 2×MIC) and PI (red, 10 μg/mL). **c** Fluorescence intensity of dye-PBGProOx$_{20}$ and PI across *S. aureus* at 1 min and 17 min. **d** Fluorescence intensity of dye-PBGProOx$_{20}$ and PI across *E. coli* at 1 min and 19 min. **e** The changes of intracellular mean fluorescent intensity with incubation time of dye-PBGProOx$_{20}$ and PI on *S. aureus* and *E. coli*. **f** Confocal images of FM4-64 stained *S. aureus* and *E. coli* after treatment with PBGProOx$_{20}$ (2×MIC) for 2 h. **g** Fluorescence changes of SYTOX in *S. aureus* and *E. coli* after treatment with PBGProOx$_{20}$ at different concentrations ($n = 3$). Data are presented as mean ± SD. SEM (**h**) and TEM (**i**) characterization of *S. aureus* and *E. coli* before (the controls) and after treatment with PBGProOx$_{20}$ (2×MIC) for 2 h.

The above results highlighted the interaction between PBGProOx$_{20}$ and the negatively charged bacterial membrane. Considering that the negative charges of bacterial membranes are primarily provided by phospholipids[58], we explored the effect of three main negatively charged bacterial phospholipids on the antibacterial potential of PBGProOx$_{20}$. Among these, phosphatidylglycerol (PG), a major anionic phospholipid in the bacterial membrane, significantly reduced the antimicrobial activity of PBGProOx$_{20}$ against both *S. aureus* and *E. coli* (Fig. 4f). Conversely, negatively charged cardiolipin (CL) and phosphatidylethanolamine (PE), along with the neutral phosphatidylcholine (PC), had little effect on the antimicrobial efficacy of PBGProOx$_{20}$ even at high concentrations (Fig. 4f, Supplementary Fig. 38). We then performed UV-vis binding study to determine the interaction between PBGProOx$_{20}$ and PG (Fig. 4g). The addition of PG induced a notable red shift in the UV-vis spectrum of PBGProOx$_{20}$, suggesting that PBGProOx$_{20}$ binds with PG to form complexes. We then quantified the binding affinity between polymers and phospholipids using isothermal titration calorimetry (ITC). The equilibrium dissociation constant (KD) between PBGProOx$_{20}$ and PG was determined to be 4.5 μmol L^{-1}, indicating a high affinity between PBGProOx$_{20}$ and the negatively charged PG (Fig. 4h); whereas, PBGProOx$_{20}$ showed poor binding affinity with neutral PC (Supplementary Fig. 39). Moreover, the KD values between PG and PNProOx$_{20}$ and between PG and PGProOx$_{20}$ were 69 μmol L^{-1} and 11 μmol L^{-1}, respectively, demonstrating that the biguanide group exhibited a substantially higher affinity for

https://doi.org/10.1038/s41467-025-67044-5

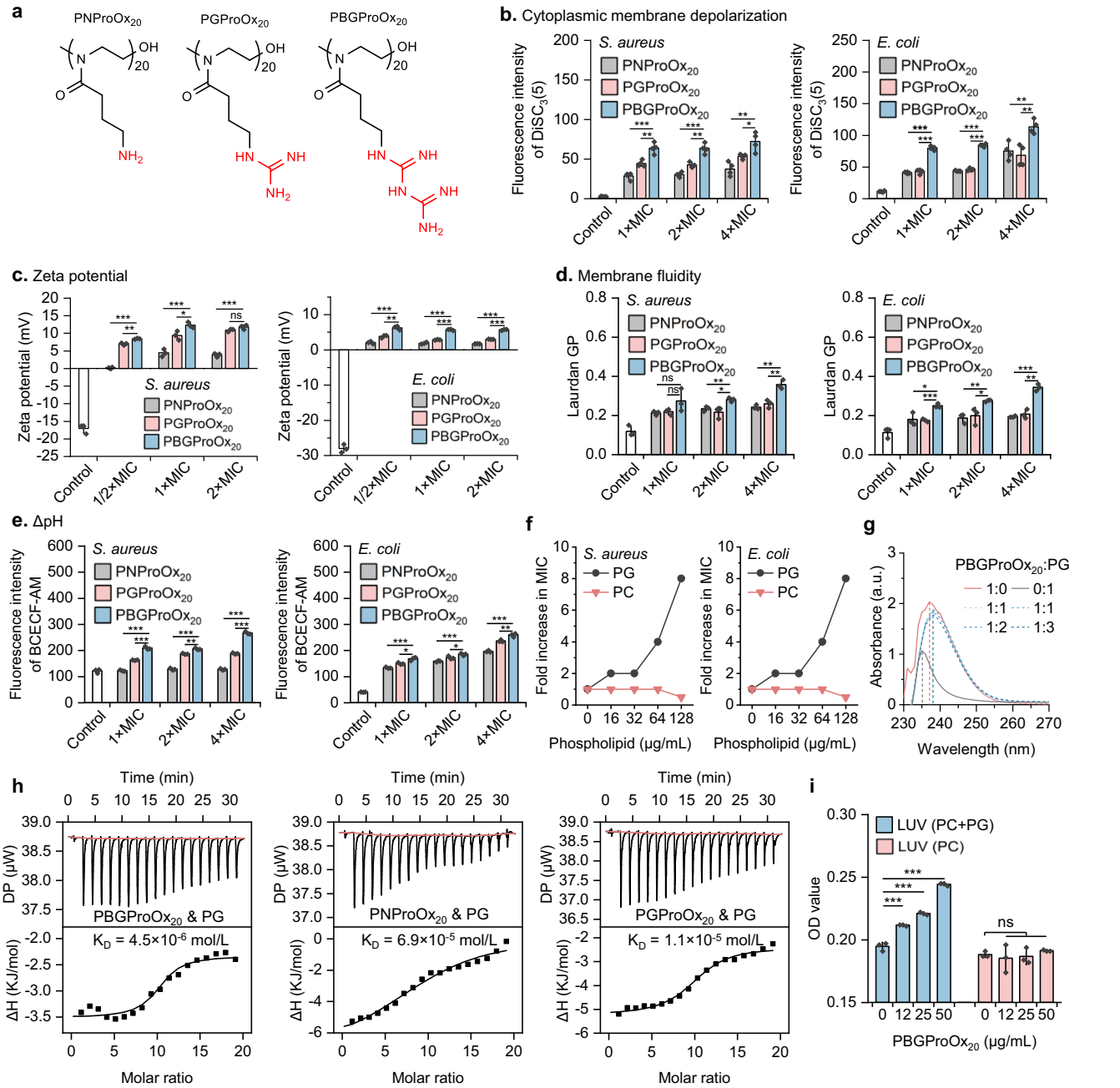

Fig. 4 | PBGProOx$_{20}$ binds more strongly with phosphatidylglycerol to damage bacterial membranes. a The structure of amine-functionalized, guanidine-functionalized and biguanide-functionalized poly(2-oxazoline)s with propyl spacer arm. **b** Cytoplasmic membrane depolarization of *S. aureus* and *E. coli* after 30-min treatment with PNProOx$_{20}$, PGProOx$_{20}$ and PBGProOx$_{20}$ at different concentrations ($n = 3$). **c** Zeta potential of *S. aureus* and *E. coli* before (the controls) and after 30-min treatment with PNProOx$_{20}$, PGProOx$_{20}$ and PBGProOx$_{20}$ at different concentrations ($n = 3$). **d** Membrane fluidity of *S. aureus* and *E. coli* before (the controls) and after 2-h treatment with PNProOx$_{20}$, PGProOx$_{20}$ and PBGProOx$_{20}$ at different concentrations ($n = 3$). **e** The dissipated ΔpH in *S. aureus* and *E. coli* before (the controls) and after 2-h treatment with PNProOx$_{20}$, PGProOx$_{20}$ and PBGProOx$_{20}$ at different concentrations ($n = 3$). **f** MIC changes of PBGProOx$_{20}$ against *S. aureus* and *E. coli* in the presence of different membrane phospholipids. **g** The UV–vis spectra of PBGProOx$_{20}$ titrated with phosphatidylglycerol (PG). **h** ITC analysis of the interaction between poly(2-oxazoline)s with different positively charged moieties and phosphatidylglycerol (PG). **i** Potassium ion leakage from large unilamellar vesicles (LUVs) with varying phospholipid compositions after 30min-treatment with PBGProOx$_{20}$ at different concentrations ($n = 3$). Data are mean ± SD in **b**–**e**, **i**. Statistical analysis was conducted using two-tailed *t*-test in **b**–**e**, **i**. $^{*}P < 0.05$, $^{**}P < 0.01$, $^{***}P < 0.001$. Exact *p* values are provided in Source Data.

negatively charged phospholipids than do amine and guanidine groups (Fig. 4h).

Large unilamellar vesicles (LUVs) composed of PG/PC (1:1) were employed to simulate bacterial membranes and figure out the interactions of PBGProOx$_{20}$ with phospholipid bilayer. PBGProOx$_{20}$ induced potassium ion leakage from these LUVs, with the extent of leakage proportional to the polymer concentration (Fig. 4i). In contrast, PBGProOx$_{20}$ exhibited virtually no effect on PC-based LUVs, which simulate mammalian cell membranes. We also found that PBGProOx$_{20}$ markedly enhanced the permeability of the outer membrane in *E. coli*, using N-Phenyl-1-naphthylamine (NPN) as the fluorescent probe (Supplementary Fig. 40). Notably, PBGProOx$_{20}$ induced the accumulation of endogenous reactive oxygen species (ROS) in treated *S. aureus* and *E. coli* (Supplementary Fig. 41). ROS may

https://doi.org/10.1038/s41467-025-67044-5

correspondingly exacerbate membrane damage, further destabilizing bacterial homeostasis. These results suggest that the biguanide moiety plays an essential role in binding phosphatidylglycerol, enabling PBGProOx$_{20}$ to disrupt the phospholipid bilayer and induce leakage of intracellular contents.

Prevention of drug resistance evolution

We subsequently evaluated whether bacteria develop antimicrobial resistance following prolonged exposure to PBGProOx$_{20}$. Neither *S. aureus* nor *E. coli* developed resistance to PBGProOx$_{20}$ after 32 passages of continuous treatment at 0.5×MIC (Fig. 5a). In contrast, under the same conditions, ciprofloxacin and moxifloxacin exhibited significant increases in MIC values against *S. aureus* (512-fold) and *E. coli* (32-fold), respectively. Furthermore, ciprofloxacin-treated *S. aureus* (*S. aureus*-ciprofloxacin-P$_{32}$) and moxifloxacin-treated *E. coli* (*E. coli*-moxifloxacin-P$_{32}$) all acquired resistance to four quinolone antibiotics and ampicillin (β-lactam antibiotic) in our study (Fig. 5b). Notably, PBGProOx$_{20}$-treated bacteria, both *S. aureus*-PBGProOx$_{20}$-P$_{32}$ and *E.*

Fig. 5 | Susceptibility of PBGProOx$_{20}$ to antimicrobial resistance and gene transcription analysis. a Drug resistance development of *S. aureus* and *E. coli* after continuous treatment with PBGProOx$_{20}$ and antibiotics at a concentration of 0.5×MIC for 32 passages. **b** MIC changes of PBGProOx$_{20}$ and different antibiotics against *S. aureus* and *E. coli*, which were treated with PBGProOx$_{20}$ and antibiotics at a concentration of 0.5×MIC for 32 passages. **c** Volcano plot of DEGs in ciprofloxacin-treated and PBGProOx$_{20}$-treated *S. aureus* compared with untreated *S. aureus*. **d** Volcano plot of DEGs in moxifloxacin-treated and PBGProOx$_{20}$-treated *E. coli* compared with untreated *E. coli*. **e** KEGG enrichment analysis of DEGs in ciprofloxacin-treated and PBGProOx$_{20}$-treated *S. aureus* compared with untreated *S. aureus*. The top 15 most enriched KEGG categories were shown in a scatter diagram in the comparison groups. **f** KEGG enrichment analysis of DEGs in moxifloxacin-treated and PBGProOx$_{20}$-treated *E. coli* compared with untreated *E. coli*. **g** Heat map of efflux pump-associated DEGs between PBGProOx$_{20}$-treated, antibiotic-treated and untreated *S. aureus* and *E. coli*. Difference clustering heatmap of regulated efflux pump genes with the treatment of PBGProOx$_{20}$ and different antibiotics. Blue, red, and white bars represent the down-regulated genes, up-regulated genes, and the genes without significant changes, respectively. **h** GO enrichment analysis of DEGs in PBGProOx$_{20}$-treated *S. aureus* compared with untreated *S. aureus*. **i** Heat map of virulence-associated DEGs between PBGProOx$_{20}$-treated and untreated *S. aureus*.

coli-PBGProOx$_{20}$-P$_{32}$, remained susceptible to all antibiotics tested (Fig. 5b). To elucidate the bacterial responses to PBGProOx$_{20}$ and antibiotic treatments, RNA-seq analysis was performed on *S. aureus* and *E. coli* following above drug resistance assays. In comparison to the *S. aureus* control group without antimicrobial treatment, the volcano plots revealed that PBGProOx$_{20}$ treatment resulted in 22 differentially expressed genes (DEGs), including 14 downregulated genes and 8 upregulated genes; whereas, ciprofloxacin treatment affected the expression of 82 DEGs, including 41 downregulated genes and 41 upregulated genes [log2-fold change ≥1; 5% fasle discovery rate (FDR)] (Fig. 5c). For *E. coli*, PBGProOx$_{20}$ treatment altered 446 DEGs, including 302 downregulated genes and 144 upregulated genes; whereas compared to *E. coli* control group without antimicrobial treatment, moxifloxacin treatment affected the expression of 795 DEGs, including 494 downregulated genes and 301 upregulated genes (Fig. 5d). The fewer DEGs observed in the PBGProOx$_{20}$ treatment group compared to antibiotic treatments suggests a lower likelihood of mutations contributing to the development of drug resistance.

Further Kyoto Encyclopedia of Genes and Genomes (KEGG) enrichment analysis was performed to categorize the gene products into standardized terms. The term Two-Component System (TCS) was identified among the top 15 enriched KEGG pathways in the ciprofloxacin-treated *S. aureus* group and moxifloxacin-treated *E. coli* group (Fig. 5e, f). TCS represents a major mechanism by which microorganisms sense and respond to external and/or intracellular stimuli by regulating the expression of genes involved in pathogenic pathways and antibiotic resistance[59]. Given the strong correlation between TCS and multidrug efflux pumps, we conducted a scan of gene expression related to various efflux pump families (Fig. 5g). Specifically, the efflux pumps genes were upregulated to varying extents in ciprofloxacin-treated *S. aureus* group, including *NorA* and *NorB* from the major facilitator super family (MFS) family, *hrtA* and *hrtB* from the ATP-binding cassette (ABC) family, *mepA* and *mepR* from the multidrug and toxic compound extrusion (MATE) family[59,60]. In the moxifloxacin-treated *E. coli* group, a large population of efflux pump genes were upregulated, including *acrA* and *acrB* from the resistance-nodulation-cell division (RND) families, *cysW* and *cysU* from the ABC family, *mdtD*, *mdtG* and *mdtL* from the MFS family[61]. In sharp contrast, almost none of the genes related to efflux pump families were upregulated in PBGProOx$_{20}$-treated groups. Conversely, PBGProOx$_{20}$ significantly downregulated several efflux pumps genes, such as *hrtA* and *hrtB* in *S. aureus*, and *mdtG* in *E. coli*. Overall, these results demonstrated that PBGProOx$_{20}$ and antibiotics exert distinct effects on the expression of drug-resistant genes, which can be attributed to their different antimicrobial mechanisms. This is also consistent with above antimicrobial resistance studies, which showed that bacteria rapidly acquired severe resistance to antibiotics, but not to PBGProOx$_{20}$.

KEGG and Gene Ontology (GO) analysis of PBGProOx$_{20}$-treated groups also revealed that the regulated pathways were mainly related to substance and energy metabolism, including amino acid biosynthesis and metabolism, fatty acid degradation and metabolism, ATPase activity, and ion transport (Fig. 5e, f, and Supplementary Figs. 42–44). These pathways are essential for bacterial survival and complex physiological functions, such as cell growth, biological production, resource uptake, and stress resistance. Besides, the expression of chemotaxis- and flagellum-related genes were significantly altered in PBGProOx$_{20}$-treated *E. coli* group, which indicated that PBGProOx$_{20}$ could regulate locomotion and adhesion of *E. coli* during pathogen-host interaction. It was also worth mentioning that the GO term related to "hemolysis in other organism" was enriched in the PBGProOx$_{20}$-treated *S. aureus* group (Fig. 5h). Bacteria often produces different virulence factors to facilitate the infections, such as leukocidins and hemolysins[62]. A further analysis showed that genes related to hemolysin including *hlgA*, *hlgB*, and *hlgC*, were significantly downregulated in PBGProOx$_{20}$-treated cells. These genes encode the gamma-hemolysin subunits HlgA, HlgB, and HlgC, respectively (Fig. 5i)[63]. Additionally, Efb and Ecb possess the ability to inhibit complement activation as well as neutrophil adhesion to fibrinogen, playing a crucial role in evading the host immune system for bacteria during colonization, spread, and distribution[60]. In present study, *Efb* and *Ecb* encoding gene *efb* and *ecb* were also significantly downregulated. Therefore, PBGProOx$_{20}$ could inhibit virulence factor secretion to reduce the inflammatory damage caused by drug-resistant bacteria, which may contribute to the in vivo therapeutic efficacy.

Broad-spectrum therapeutic efficacy of PBGProOx$_{20}$ in mice models of local and systemic bacterial infections

In light of the potent in vitro antimicrobial performance of PBGProOx$_{20}$, we further investigated the in vivo therapeutic efficacy using multiple mice models. In the mice models of full-thickness wound infections (Fig. 6a), saline-treated wounds showed bacterial burdens with 7.6 log CFU/g for *S. aureus* and 8.9 log CFU/g for *E. coli* (Fig. 6b). The topical application of PBGProOx$_{20}$ achieved 2.2 and 2.6 logs reduction of *S. aureus* and *E. coli*, respectively, in the infected wounds, which outperformed vancomycin (1.2 logs reduction) and imipenem (2.1 logs reduction). In the mice models of subcutaneous infections, bacterial loads in the infected skin exceeded 10 log CFU/g. PBGProOx$_{20}$ treatment led to a reduction of more than 1 log CFU/g for both *S. aureus* and *E. coli*, showing efficacy comparable to colistin but surpassing that of vancomycin (less than 0.5 log reduction) (Fig. 6c, d).

We further evaluated the anti-infective efficacy of PBGProOx$_{20}$ in a mice models of renal infections induced by *S. aureus* and *E. coli* (Fig. 6e). Systemic administration with PBGProOx$_{20}$ significantly decreased the bacterial loads in the infected kidneys from 7 log CFU/g to 4.6 log CFU/g for *S. aureus*, and from 8.5 log CFU/g to 5.5 log CFU/g for *E. coli* (Fig. 6f). Besides, PBGProOx$_{20}$ substantially alleviated necrosis in the glomeruli and renal tubules, and improved the condition of renal lesions (Fig. 6g). In addition, the therapeutic efficacy of PBGProOx$_{20}$ was also evaluated in a mice models of peritonitis (Fig. 7a). Intraperitoneal injection with four different bacterial suspensions resulted in 100% death of mice within 3 days (Fig. 7b). A single dose of PBGProOx$_{20}$ significantly improved survival rates, rescuing 83% of *S. aureus* infected mice, as well as 100% of the mice infected with *S. epidermidis*, *E. coli*, and *A. baumannii*. Furthermore, PBGProOx$_{20}$ treatments significantly reduced bacterial loads within the blood, peritoneal fluid and major organs, including heart, liver, spleen, lung,

https://doi.org/10.1038/s41467-025-67044-5

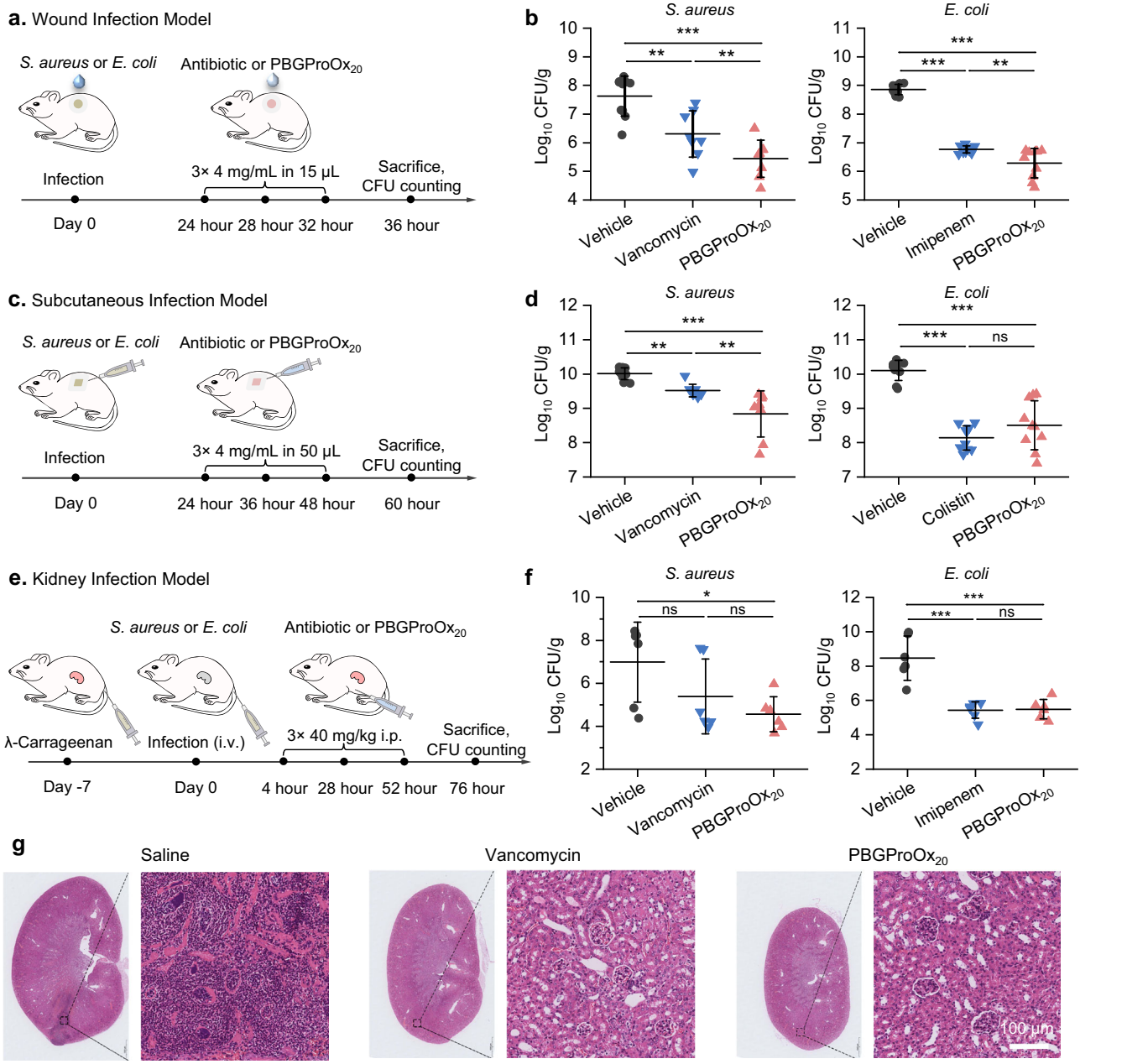

Fig. 6 | In vivo anti-infectious efficacy of PBGProOx$_{20}$ in mice models of full-thickness infections, subcutaneous infections, and kidney infections. **a** Schematic representation of the full-thickness infection model. The infected wounds were treated topically with 15 μL of saline, PBGProOx$_{20}$ (4 mg/mL), vancomycin (4 mg/mL) or imipenem (4 mg/mL) every 4 h for triple applications. **b** Bacterial load of the mice wound after treatment with saline, PBGProOx$_{20}$, vancomycin or imipenem in the full-thickness infection model induced by *S. aureus* and *E. coli*, respectively. Each point represents one wound sample ($n = 10$). **c** Schematic representation of the subcutaneous infection model. The infected tissues were treated subcutaneously with 100 μL of saline, PBGProOx$_{20}$ (4 mg/mL), vancomycin (4 mg/mL) or colistin (4 mg/mL) every 12 h for triple applications. **d** Bacterial load of the mice skin after treatment with saline, PBGProOx$_{20}$, vancomycin or colistin in the subcutaneous infection model induced by *S. aureus* and *E. coli*, respectively. Each point represents one skin sample ($n = 6$). **e** Schematic representation of the kidney infection model. The infected mice were treated intraperitoneally with saline, PBGProOx$_{20}$ (40 mg/kg), vancomycin (40 mg/kg) or imipenem (40 mg/kg) daily for triple applications. **f** Bacterial load of the mice kidney after treatment with saline, PBGProOx$_{20}$, vancomycin or imipenem in the kidney infection model induced by *S. aureus* and *E. coli*, respectively. Each point represents one kidney sample ($n = 6$). **g** Histological analysis by H&E staining of kidney sections from the *S. aureus*-infected mice after treatment with saline, vancomycin and PBGProOx$_{20}$. Data are presented as mean ± SD in **b**, **d**, **f**. Statistical analysis was conducted using one-way ANOVA with multiple comparisons using Tukey's post-test in **b**, **d**, **f**. $^{*}P < 0.05$, $^{**}P < 0.01$, $^{***}P < 0.001$. Exact p values are provided in Source Data.

and kidney. The demonstrated therapeutic efficacy was comparable to or even superior to that of vancomycin and imipenem (Fig. 7c–f). Histological examination of major organs through hematoxylin and eosin (H&E) staining revealed that PBGProOx$_{20}$ treatments effectively mitigated organ lesions, including hepatocyte necrosis, loss of splenic white pulp, alveolar wall thickening, and glomerular necrosis (Fig. 7g).

Cell-penetrating and BBB-penetrating properties of PBGProOx$_{20}$

We further used rhodamine-labelled polymer (RB-PBGProOx$_{20}$, red fluorescence) to explore the cell-penetrating behavior of PBGProOx$_{20}$ in brain microvascular endothelial cells (bEnd.3) (Supplementary Figs. 35b and 36b). The obvious increase in intracellular fluorescence

https://doi.org/10.1038/s41467-025-67044-5

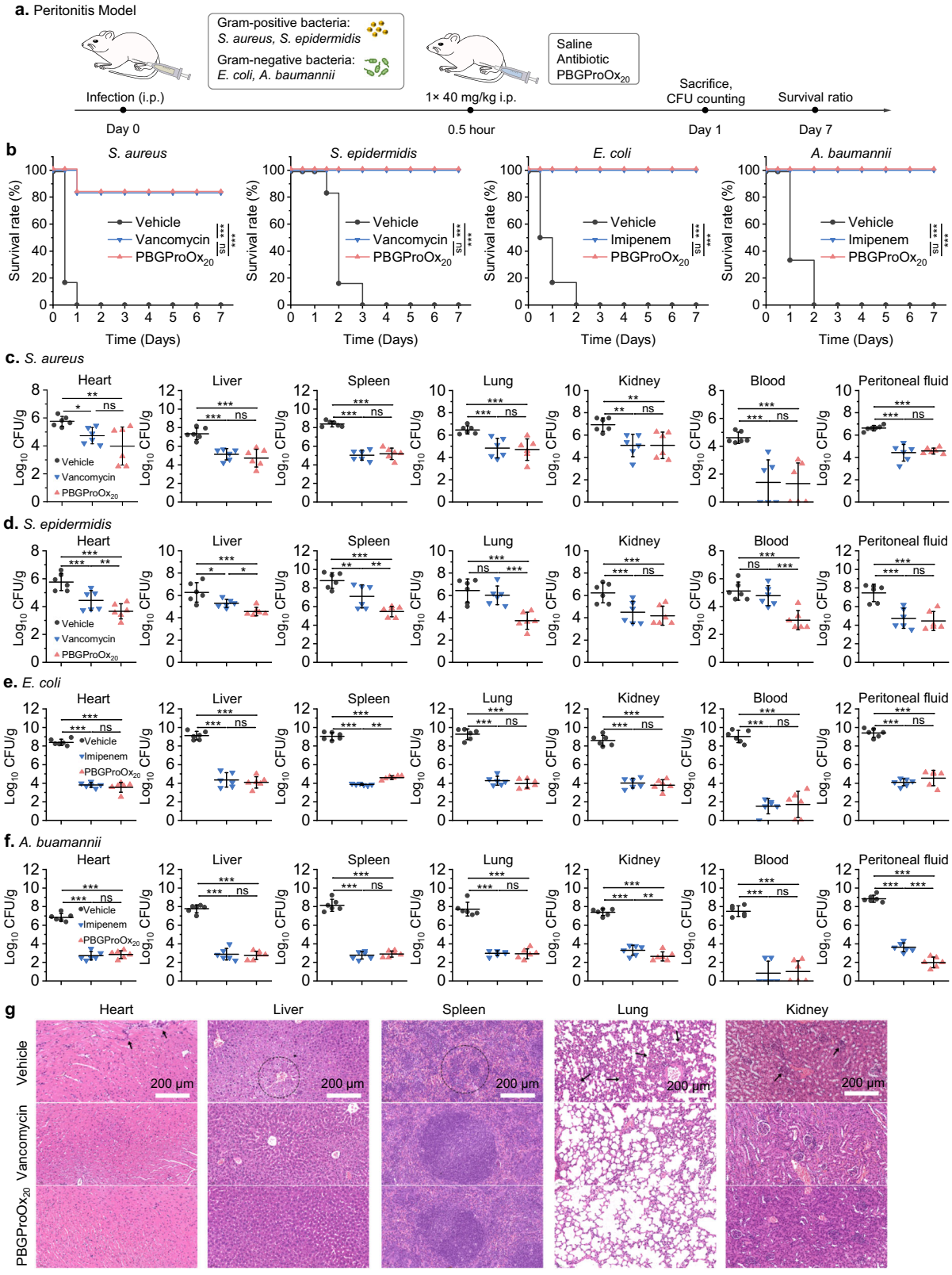

over time suggested efficient internalization of $PBGProOx_{20}$ toward bEnd.3 cells (Fig. 8a). Live-cell fluorescence imaging showed that $PBGProOx_{20}$ predominantly localized within the endolysosomal compartments, rather than in mitochondria (Fig. 8b), which prevents interaction between $PBGProOx_{20}$ and mitochondria, contributing to the low cytotoxicity. Considering that the mitochondrial membrane also contains negatively charged phospholipids, the mitochondrial membrane potential was also characterized using rhodamine 123 (Supplementary Fig. 45). It was found that the mitochondrial membrane potential in bEnd.3 cells remained normal after $PBGProOx_{20}$ treatment, which further ruled out any adverse effects of $PBGProOx_{20}$ on mitochondria.

To figure out the cellular uptake mechanism of $PBGProOx_{20}$, we compared the internalization of $PBGProOx_{20}$ in bEnd.3 cells at both

https://doi.org/10.1038/s41467-025-67044-5

Fig. 7 | In vivo anti-infectious efficacy of PBGProOx$_{20}$ in a mice model of peritonitis. a Schematic representation of the peritonitis model. The infected mice were treated intraperitoneally with saline, PBGProOx$_{20}$ (40 mg/kg), vancomycin (40 mg/kg) or imipenem (40 mg/kg) for once application. **b** Survival rates of infected mice after treatment with saline, PBGProOx$_{20}$, vancomycin or imipenem in the peritonitis model ($n = 6$). The mice were infected by *S. aureus*, *S. epidermidis*, *E. coli* and *A. baumannii*, respectively. The survival benefit was determined using a log-rank test. $^{**}P < 0.01$, $^{***}P < 0.001$. Bacterial load in different organs, blood, and peritoneal fluid in the peritonitis model induced by *S. aureus* (**c**), *S. epidermidis* (**d**), *E. coli* (**e**) and *A. baumannii* (**f**), respectively ($n = 6$). **g** Histological analysis by H&E staining of various organs sections from the *S. aureus*-infected mice after the treatment with saline, vancomycin and PBGProOx$_{20}$. Black arrows and circles represent histological anomalies. Data are presented as mean ± SD in **c**–**f**. Statistical analysis was conducted using one-way ANOVA with multiple comparisons using Tukey's post-test in **c**–**f**. $^{*}P < 0.05$, $^{**}P < 0.01$, $^{***}P < 0.001$. Exact *p* values are provided in Source Data.

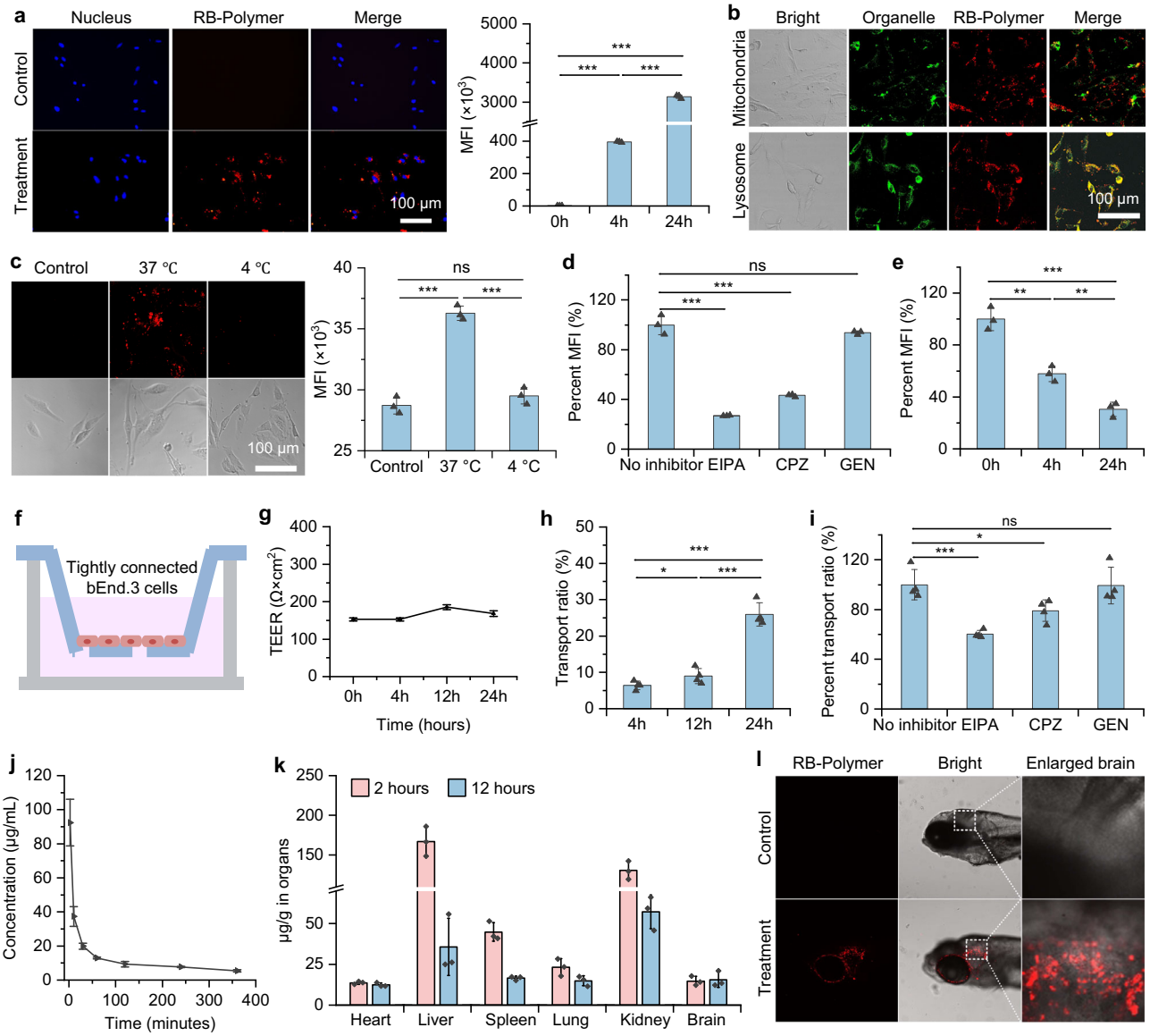

Fig. 8 | Cell-penetrating and BBB-penetrating properties of PBGProOx$_{20}$. **a** Fluorescent images (left) and flow cytometry analyses (right, $n = 3$) on mean fluorescence intensity (MFI) of bEnd.3 cells before and after treatment with RB-PBGProOx$_{20}$ (12.5 μg/mL). **b** Mitochondrial and lysosomal colocalization in bEnd.3 cells after treatment with RB-PBGProOx$_{20}$ (12.5 μg/mL) for 4 h. **c** Confocal images (left) and flow cytometry analyses (right, $n = 3$) of bEnd.3 cells after treatment with RB-PBGProOx$_{20}$ (12.5 μg/mL) at 37 °C and 4 °C. **d** Percent uptakes of the RB-PBGProOx$_{20}$ (12.5 μg/mL) within 4 h in bEnd.3 cells pre-treated with different endocytosis inhibitors, including 5-(N-Ethyl-N-isopropyl)-Amiloride (EIPA), chlorpromazine (CPZ) and genistein (GEN) ($n = 3$). **e** Flow cytometry analyses of RB-PBGProOx$_{20}$-treated bEnd.3 cells after different exocytosis time ($n = 3$). **f** Schematic representation of the in vitro transwell model. **g** TEER values of bEnd.3 cells monolayer in the transwell model after treatment with RB-PBGProOx$_{20}$ (12.5 μg/mL) at different time points ($n = 4$). **h** The transport ratio of RB-PBGProOx$_{20}$ in the transwell model after different incubation time ($n = 4$). **i** Percent transport ratio of RB-PBGProOx$_{20}$ in the transwell model at the presence of different endocytosis inhibitors ($n = 4$). **j** Curves of plasma concentrations of RB-PBGProOx$_{20}$ over time after administration of 20 mg/kg via intraperitoneal injection ($n = 3$). **k** In vivo distribution of RB-PBGProOx$_{20}$ in mice organs after administration of 20 mg/kg via intraperitoneal injection ($n = 3$). **l** Confocal images of the zebrafish larvae before (Control) and after systemic administration of RB-PBGProOx$_{20}$ (3.13 μg/mL) for 1 h. Data are presented as mean ± SD in **a**, **c**–**e**, **g**–**k**. Statistical analysis was conducted using one-way ANOVA with multiple comparisons using Tukey's post-test in **a**, **c**, **e**, **h**; Statistical analysis was conducted using two-tailed *t*-test in **d**, **i**. $^{*}P < 0.05$, $^{**}P < 0.01$, $^{***}P < 0.001$. Exact *p* values are provided in Source Data.

4 °C and 37 °C. The absence of the RB-PBGProOx$_{20}$ fluorescent signal at 4 °C suggested that the internalization of PBGProOx$_{20}$ relies on energy-dependent endocytosis, rather than energy-independent direct penetration (Fig. 8c). Endocytosis can occur through various pathways, including macropinocytosis, clathrin-dependent endocytosis, and caveolin-dependent endocytosis[42]. We then blocked these pathways individually with different inhibitors to further explore the specific endocytosis pathway of PBGProOx$_{20}$. Ethylisopropylamiloride (EIPA) and chlorpromazine (CPZ), but not genistein (GEN), significantly inhibited the cellular uptake of PBGProOx$_{20}$ in bEnd.3 cells, indicating that macropinocytosis and clathrin-dependent endocytosis together dominate the internalization of PBGProOx$_{20}$ (Fig. 8d). Furthermore, we observed an obvious exocytosis process of PBGProOx$_{20}$ in bEnd.3 cells over time (Fig. 8e). This continuous transcytosis behavior further underscores the potential of PBGProOx$_{20}$ to penetrate BBB.

The in vitro transwell model was further used to quantify the BBB-penetrating efficiency of PBGProOx$_{20}$ (Fig. 8f). The initial transendothelial electrical resistance (TEER) values in transwell model exceeded 150 Ω·cm^2, indicating tight junctions of bEnd.3 cells (Fig. 8g)[64]. Notably, PBGProOx$_{20}$ did not disrupt the tight junctions of bEnd.3 cells, as TEER values remained stable in the presence of PBGProOx$_{20}$. Importantly, PBGProOx$_{20}$ exhibited an increased transport ratio over incubation time, reaching ~26% after 24 h (Fig. 8h). Moreover, the transport ratio of PBGProOx$_{20}$ in the transwell model was inhibited by EIPA and CPZ in a manner consistent with the results of cellular uptake study (Fig. 8i). These findings demonstrated that PBGProOx$_{20}$ could effectively penetrate the BBB through a transcytosis process, which involved macropinocytosis and clathrin-dependent endocytosis, and subsequent exocytosis.

The promising in vitro cell-penetrating capabilities of PBGProOx$_{20}$ prompted us to explore the in vivo BBB-penetrating ability. We investigated the plasma pharmacokinetics of RB-PBGProOx$_{20}$ using fluorescent quantification method. Following a 20-mg/kg bolus dose, the plasma concentrations of PBGProOx$_{20}$ achieved were above those required for antimicrobial activity in vitro and a half-life of ~4 h was defined (Fig. 8j, and Table S8). After systemic administration in mice, PBGProOx$_{20}$ was found with significant amount within the brain, showing distribution levels comparable to that in the heart, spleen, and lung (Fig. 8k). The in vivo BBB-penetrating ability of PBGProOx$_{20}$ was further confirmed using the well-established zebrafish model by observing obvious fluorescence signal in the zebrafish brain region after administration with RB-PBGProOx$_{20}$ (Fig. 8l)[65]. These results altogether demonstrated the ability of PBGProOx$_{20}$ to penetrate the BBB, showing potential in treating bacterial meningitis caused by ESKAPE pathogens.

Broad-spectrum and potent antimicrobial efficacy in bacterial meningitis and low in vivo toxicity of PBGProOx$_{20}$

Bacterial suspensions of *S. aureus* and *E. coli* were directly injected into mice brains to induce bacterial meningitis (Fig. 9a). The saline-treated mice all showed a poor survival rate of 17%. Systemic administrations with PBGProOx$_{20}$ significantly improved survival rates, rescuing 83% of both *S. aureus*-infected and *E. coli*-infected mice (Fig. 9b), superior to that of vancomycin (50%) on *S. aureus*-infected mice but slightly inferior to that of meropenem (100%) on *E. coli*-infected mice. Quantitative analysis of the bacterial load in the mice brain indicated that saline-treated mice showed high bacterial burdens, with 8.0 log CFU/brain for *S. aureus* and 8.9 log CFU/brain for *E. coli* (Fig. 9c). PBGProOx$_{20}$ treatment led to a 2 log and 4.1 log decrease in bacterial loads for *S. aureus* and *E. coli*, respectively, which was superior to that of vancomycin and comparable to that of meropenem. Histological examination through H&E staining revealed that PBGProOx$_{20}$ treatments effectively mitigated inflammation of the infected brain, especially infiltration of neutrophils (Fig. 9d).

We also conducted a single-dose tolerability study to evaluate the in vivo biosafety of PBGProOx$_{20}$. After intraperitoneal injection with high dose (200 and 300 mg/kg) of PBGProOx$_{20}$, the mice demonstrated 100% survival without any sign of malaise within 14 days. PBGProOx$_{20}$ at 400 mg/kg caused 33% death and the maximum tolerated dose (MTD) of PBGProOx$_{20}$ was determined to be ~300 mg/kg (Fig. 9e). PHMB exhibited stronger systemic toxicity, with a MTD of ~20 mg/kg, making it difficult to meet the biosafety requirements for in vivo infection treatment. Moreover, the normal increase in mice body weight was also observed over a 14-day period post-administration with PBGProOx$_{20}$ (Fig. 9f). The immunohistology analysis of the liver and kidney at 2 days and 14 days post injection showed that PBGProOx$_{20}$ caused little toxicity to organs critical for metabolism (Fig. 9g). Further investigations into the complete blood count revealed that hematological parameters in PBGProOx$_{20}$-treated mice were consistent with those observed in saline-treated mice, encompassing red blood cell count (RBC), white blood cell count (WBC), and platelet count (PLT) counts (Fig. 9h). Besides, the blood biochemical parameters also remained within normal ranges, including liver function indicators (aspartate aminotransferase (AST) and alanine aminotransferase (ALT)), renal function indicators (blood urea nitrogen (BUN) and creatinine (CREA)), and electrolyte balance (potassium (K^+), sodium (Na^+), and chloride (Cl^-)) (Fig. 9h). These findings collectively demonstrate the biosafety of PBGProOx$_{20}$ for systemic administration, particularly in treating bacterial meningitis.

Discussion

Positively charged moieties have been widely recognized as critical parameters in HDP and their mimics. These cationic compounds selectively target bacterial membranes that have abundant anionic phospholipids via electrostatic interactions. Currently, amine and guanidine are the main positively charged moieties for designing HDP mimics with positive charges that are provided by lysine and arginine residues. Besides, guanidine-functionalized compounds inspired by cell-penetrating peptides have been demonstrated to penetrate the BBB to effectively treat meningitis. To find an effective HDP mimic designing strategy to combat drug-resistant ESKAPE pathogens and bacterial meningitis, we focused on the biguanide group that possess higher positively charged density and stronger interactions with anionic phospholipids on bacterial membranes.

Based on the biguanide-functionalized designing strategy, the optimal HDP-mimicking poly(2-oxazoline)s, PBGProOx$_{20}$, exhibits potent and selective antimicrobial activity against drug-resistant bacteria, including multiple clinically isolated ESKAPE pathogens. PBGProOx$_{20}$ also demonstrates potent activities to kill persisters and eradicate mature biofilms. Due to the phosphatidylglycerol-targeting antimicrobial mechanism, PBGProOx$_{20}$ disrupts the integrity of bacterial membrane, without inducing antimicrobial resistance and cross-resistance even after continuous treatment. It is noteworthy that PBGProOx$_{20}$ does not induce any upregulation of drug resistance-related genes from various efflux pump families. Besides, PBGProOx$_{20}$ downregulates the expression of genes related to virulence factors, potentially enhancing its in vivo efficacy against bacterial infections. PBGProOx$_{20}$ shows promising therapeutic efficacy in mice models of full-thickness infections, subcutaneous infections, kidney infections and peritonitis, without showing systemic toxicity. PBGProOx$_{20}$ also exhibits continuous transcytosis behavior within brain microvascular endothelial cells, along with substantial penetrating efficiency in tanswell model. Consequently, PBGProOx$_{20}$ effectively penetrated the BBB to distribute in the brain tissues of mice and zebrafish, achieving potent therapeutic efficacy in treating drug-resistant bacterial meningitis.

Our study provides an alternative designing option of the positively charged moiety to develop potent antimicrobial and BBB-penetrating HDP mimics. PBGProOx$_{20}$ holds promise as a potential therapeutic against life-threatening drug-resistant systemic infections and CNS infections like meningitis, particularly where conventional

https://doi.org/10.1038/s41467-025-67044-5

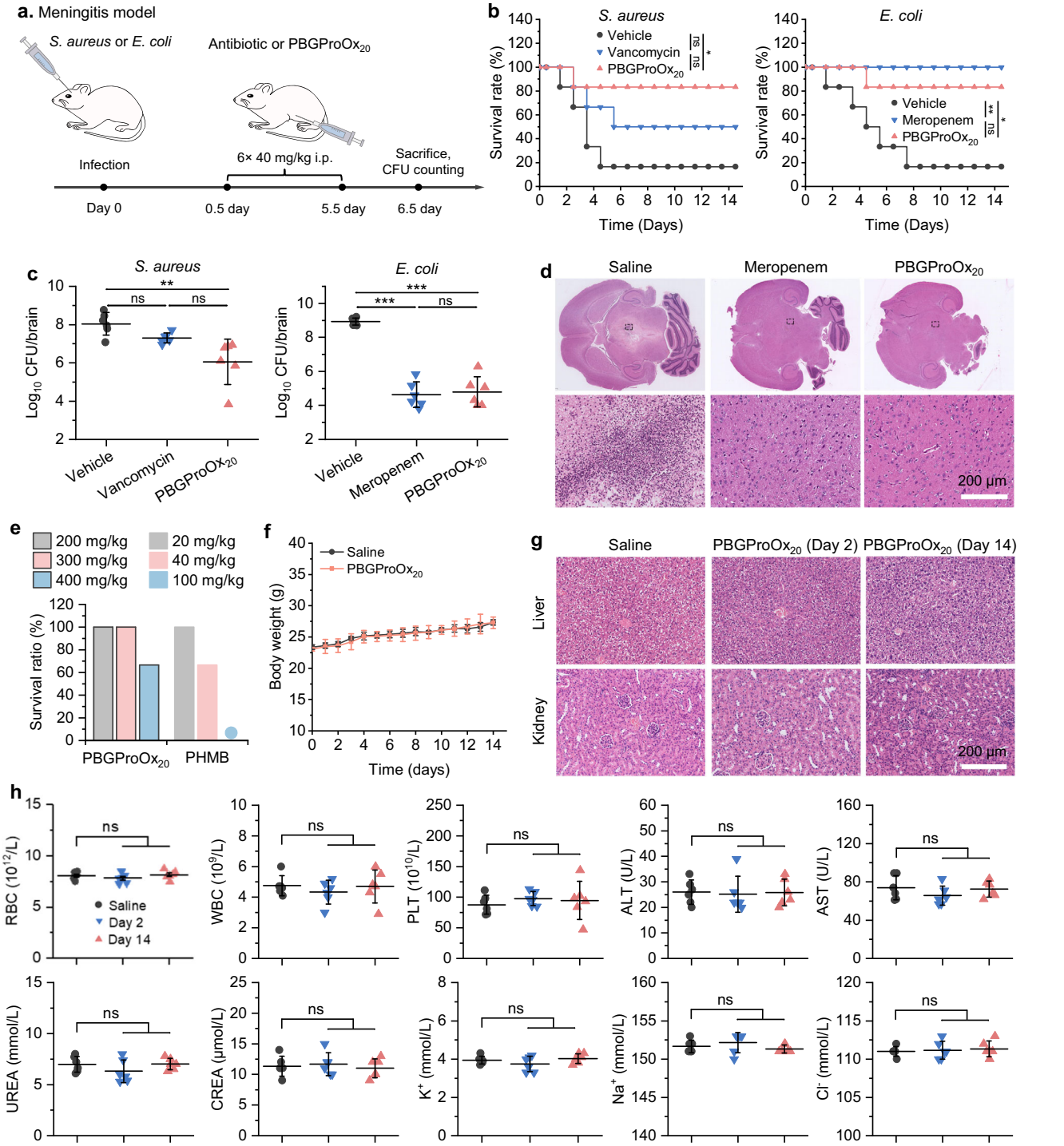

Fig. 9 | In vivo anti-infectious efficacy of PBGProOx$_{20}$ in the mice model of meningitis and in vivo toxicity. a Schematic representation of the meningitis model. The infected mice were treated intraperitoneally with saline, PBGProOx$_{20}$ (40 mg/kg), vancomycin (40 mg/kg) or meropenem (40 mg/kg) daily for six applications. **b** Survival rates of infected mice after treatment with saline, PBGProOx$_{20}$, vancomycin or imipenem in the meningitis model ($n = 6$). The mice were infected by *S. aureus* and *E. coli*, respectively. The survival benefit was determined using a log-rank test. $^{*}P < 0.05$, $^{***}P < 0.01$, $^{***}P < 0.001$. **c** Bacterial load of the mice brain infected by *S. aureus* and *E. coli*, respectively, with and without antimicrobial treatment in the meningitis models ($n = 6$). Statistical analysis was conducted using one-way ANOVA with multiple comparisons using Tukey's post-test. $^{*}P < 0.05$, $^{**}P < 0.01$, $^{***}P < 0.001$. **d** Histological analysis by H&E staining of mice brain from the *E. coli*-infected mice after the treatment with saline, meropenem and PBGProOx$_{20}$. **e** Survival rates of the uninfected mice at day 14 after the single-dose intraperitoneal injection of PBGProOx$_{20}$ and poly(hexamethylene biguanide) (PHMB) at different concentrations ($n = 6$). **f** Body weight changes of mice after the single-dose intraperitoneal injection of saline and PBGProOx$_{20}$ (40 mg/kg), respectively ($n = 6$). **g** H&E staining analysis at day 2 and day 14 on kidney and liver from the mice after the single-dose intraperitoneal injection with saline and PBGProOx$_{20}$ (40 mg/kg), respectively. **h** Hematological parameters analysis at day 2 and day 14 on the mice after the single-dose intraperitoneal injection with saline and PBGProOx$_{20}$ (40 mg/kg), respectively ($n = 6$). Statistical analysis was conducted using two-tailed *t*-test. Data are presented as mean ± SD in **c**, **f**, **h**. Exact *p* values are provided in Source Data.

antibiotics fail. However, realizing this clinical potential will require further exploration, including scalable synthesis, comprehensive long-term toxicity profiling, and detailed pharmacokinetic/pharmacodynamic optimization. Furthermore, developing stable formulations suitable for corresponding administration routes will be critical for clinical translation. Beyond $PBGProOx_{20}$, the biguanide design paradigm provides a robust platform for developing next-generation antimicrobials against a wider spectrum of multi-drug resistant pathogens, while its BBB-penetrating efficacy opens avenues for treating other CNS infections or repurposing as a neurotherapeutic delivery platform. Future research will focus on investigating how cationic and hydrophobic groups affect the BBB-penetrating efficiency, and exploring diverse molecular structures to enhance antimicrobial potency and BBB penetration efficiency.

Methods

All animal research was performed in accordance with the Guidelines for Care and Use of Laboratory Animals of East China University of Science and Technology. All procedures in this study were approved by the Animal Research Bioethics Committee, East China University of Science and Technology (ECUST-2023-012). Mice were raised in an individually ventilated cage (IVC) system at 20–26 °C and 40–70% humidity, with a dark/light cycle of 12 h.

Mice wound infection model

This model was conducted according to the previously reported method with slight modification[66]. Female ICR mice (6–8 weeks) were anesthetized with an intraperitoneal injection of sodium pentobarbital at a dose of 75 mg/kg and the hair on the mice back was shaved. *S. aureus* USA300 LAC or *E. coli* ATCC25922 were cultured in LB medium at 37 °C for 9 h, then collected and suspended in saline at a cell density of 3×10^6 CFU/mL or 1×10^8 CFU/mL, respectively. The full-thickness wounds (6-mm diameter) were obtained using biopsy punch, and bacterial suspensions were dropped to wound sites. After 24-h post infection, 15 μL saline containing $PBGProOx_{20}$ (4 mg/mL), vancomycin (4 mg/mL for treatment of *S. aureus* infection) or imipenem (4 mg/mL for treatment of *E. coli* infection) was applied to the infected wounds. Saline treatment was used as the control. The treatment was conducted every 4 h for a total of 3 times. The treated wound sites were excised for CFU quantification of bacterial load at 4 h after the last treatment ($n = 10$ in each group).

Mice subcutaneous infection model

This model was conducted according to the previously reported method with slight modification[67]. Female ICR mice (6–8 weeks) were anesthetized with an intraperitoneal injection of sodium pentobarbital at a dose of 75 mg/kg and the hair on the mice back was shaved. *S. aureus* USA300 LAC or *E. coli* ATCC25922 were cultured in LB medium at 37 °C for 9 h, then collected and suspended in saline at a cell density of 1.5×10^9 CFU/mL or 1.5×10^8 CFU/mL, respectively. 100 μL of bacterial suspensions were injected into the subcutaneous area of the mice back. After 24-h post infection, 50 μL saline containing $PBGProOx_{20}$ (4 mg/mL), vancomycin (4 mg/mL for treatment of *S. aureus* infection) or colistin (4 mg/mL for treatment of *E. coli* infection) was applied to the infected sites through subcutaneous injection. Saline treatment was used as the control. The treatment was conducted every 12 h for a total of 3 times. The treated wound sites were excised for CFU quantification of bacterial load at 12 h after the last treatment ($n = 10$ in each group).

Mice kidney infection model

This model was conducted according to the previously reported method with slight modification[68]. Female ICR mice (6–8 weeks) were intravenously injected with 0.2 mL carrageenan solution (2 mg/mL) at 7 days prior to infection. *S. aureus* USA300 LAC or *E. coli* ATCC25922 were cultured in LB medium at 37 °C for 9 h, then collected and suspended in saline at a cell density of 1.5×10^7 CFU/mL or 6×10^7 CFU/mL, respectively. 200 μL of bacterial suspensions were intravenously injected into above mice. After 4-h post infection, saline containing $PBGProOx_{20}$ (40 mg/kg), vancomycin (40 mg/kg for treatment of *S. aureus* infection) or imipenem (40 mg/kg for treatment of *E. coli* infection) was intraperitoneally injected into the infected mice. Saline treatment was used as the control. The treatment was conducted every 24 h for a total of 3 times. The mice kidneys were excised for CFU quantification of bacterial load and histological analysis at 24 h after the last treatment ($n = 6$ in each group).

Mice peritonitis models

This model was conducted according to the previously reported method with slight modification[27,69]. *S. aureus* USA300 LAC, *S. epidermidis* 9397, *E. coli* 2904 and *A. baumannii* 0403 were cultured in LB medium at 37 °C for 9 h, then collected and suspended in 5% mucin solution at a cell density of 7.5×10^8 CFU/mL, 5.1×10^9 CFU/mL, 2×10^5 CFU/mL or 5×10^6 CFU/mL, respectively. For *S. epidermidis*-induced peritonitis model, female ICR mice (6–8 weeks) were immunosuppressed by intraperitoneal injection of cyclophosphamide (150 mg/kg) at 4 days and cyclophosphamide (100 mg/kg) at 1 day prior to infection. The mice used in other bacteria-induced peritonitis models were normal. 200 μL of bacterial suspensions were intraperitoneally injected into female ICR mice (6–8 weeks). After 30-min post infection, saline containing $PBGProOx_{20}$ (40 mg/kg), vancomycin (40 mg/kg for treatment of *S. aureus* and *S. epidermidis* infections) or imipenem (40 mg/kg for treatment of *E. coli* and *A. baumannii* infections) was intraperitoneally injected into the infected mice. Saline treatment was used as the control. The mice organs were excised for quantification of bacterial load and histological analysis at 24 h after the infection and the survival of remaining mice was recorded for 7 days ($n = 6$ in each group).

Mice meningitis models

This model was conducted according to the previously reported method with slight modification[70]. Female ICR mice (6–8 weeks) were anesthetized with an intraperitoneal injection of sodium pentobarbital at a dose of 75 mg/kg and the hair on the mice head was shaved. *S. aureus* USA300 LAC and *E. coli* ATCC25922 were cultured in LB medium at 37 °C for 9 h, then collected and suspended in saline at a cell density of 2.5×10^7 CFU/mL or 1.6×10^6 CFU/mL, respectively. Female mice were infected intraventricularly (20 μL of bacterial suspensions) via a burr hole (coordinates 0.6 mm dorsal to bregma, 1.2 mm lateral to middle line and 2 mm ventral). After 12-h post infection, saline containing $PBGProOx_{20}$ (40 mg/kg), vancomycin (40 mg/kg for treatment of *S. aureus* infections) or meropenem (40 mg/kg for treatment of *E. coli* infections) was intraperitoneally injected into the infected mice. Saline treatment was used as the control. The treatment was conducted every 24 h for a total of 6 times. The mice brains were excised for quantification of bacterial load and histological analysis at 24 h after the last treatment, and the survival of remaining mice was recorded for 14.5 days ($n = 6$ in each group).

In vivo toxicity evaluation on $PGMeOx_{10}$

In mice dose tolerance study, female ICR mice (6–8 weeks) were intraperitoneally administered with $PBGProOx_{20}$ (200 mg/kg, 300 mg/kg, and 400 mg/kg) and PHMB (20 mg/kg, 40 mg/kg, and 100 mg/kg). The survival of treated mice was recorded for 14 days after the first treatment ($n = 6$ in each group). The body weight of mice treated with $PBGProOx_{20}$ (40 mg/kg) were recorded until 14 days after the first treatment, and the mice blood were collected at 2 days or 14 days after the first treatment for complete blood count and blood biochemical parameters analysis, including red blood cell count (RBC), white blood cell count (WBC), and platelet count (PLT), aspartate

alanine aminotransferase (ALT), aminotransferase (AST), blood urea nitrogen (BUN), creatinine (CREA), and three ions (K^+, Na^+, Cl^-). The mice liver and kidney were also excised for histological analysis. Saline treatment was used as the control.

Statistical analysis

Statistical analysis was performed using Origin software. Significance analysis between two groups were performed using two-tailed student's *t*-test. Significance analysis for multiple comparison of more than two groups were performed using one-way analysis of variance of (ANOVA) with Turkey post-test. All mean ± standard deviation was indicated by the error bars. The differences were regarded as statistically not significant (ns) with probability $P > 0.05$ and significant with probability $P < 0.05$ ($^{*}P < 0.05$, $^{**}P < 0.01$, $^{***}P < 0.001$).

Reporting summary

Further information on research design is available in the Nature Portfolio Reporting Summary linked to this article.

Data availability

All data generated in this study are provided in the Supplementary Information/Source Data file. All data underlying this study are available from the corresponding author upon request. Source data are provided with this paper.

Code availability

The RNA-seq data generated in this study have been deposited in the National Center for Biotechnology Information (NCBI) database under accession code PRJNA1311716.

References

1. Hasbun, R. Progress and challenges in bacterial meningitis: a review. *JAMA* **328**, 2147–2154 (2022).
2. Willyard, C. The drug-resistant bacteria that pose the greatest health threats. *Nature* **543**, 15–15 (2017).
3. Oliveira, D. M. P. D. et al. Antimicrobial resistance in ESKAPE pathogens. *Clin. Microbiol. Rev.* **33**, https://doi.org/10.1128/cmr.00181-00119 (2020).
4. Wu, D. et al. The blood–brain barrier: structure, regulation, and drug delivery. *Sig. Transduct. Target. Ther.* **8**, 217 (2023).
5. de Breij, A. et al. The antimicrobial peptide SAAP-148 combats drug-resistant bacteria and biofilms. *Sci. Transl. Med.* **10**, eaan4044 (2018).
6. Hancock, R. E. W., Alford, M. A. & Haney, E. F. Antibiofilm activity of host defence peptides: complexity provides opportunities. *Nat. Rev. Microbiol.* **19**, 786–797 (2021).
7. Lazzaro, B. P., Zasloff, M. & Rolff, J. Antimicrobial peptides: application informed by evolution. *Science* **368**, eaau5480 (2020).
8. Huang, J. et al. Identification of potent antimicrobial peptides via a machine-learning pipeline that mines the entire space of peptide sequences. *Nat. Biomed. Eng.* **7**, 797–810 (2023).
9. Porter, E. A., Wang, X., Lee, H.-S., Weisblum, B. & Gellman, S. H. Non-haemolytic β-amino-acid oligomers. *Nature* **404**, 565–565 (2000).
10. Botelho Sampaio de Oliveira, K., Lopes Leite, M., Albuquerque Cunha, V., Brito da Cunha, N. & Luiz Franco, O. Challenges and advances in antimicrobial peptide development. *Drug Discov. Today* **28**, 103629 (2023).
11. Kurnaz, L. B. et al. Facial amphiphilic naphthoic acid-derived antimicrobial polymers against multi-drug resistant gram-negative bacteria and biofilms. *Biomaterials* **301**, 122275 (2023).
12. Lee, E. Y. et al. PACAP is a pathogen-inducible resident antimicrobial neuropeptide affording rapid and contextual molecular host defense of the brain. *Proc. Natl. Acad. Sci. USA* **118**, e1917623117 (2021).
13. dos Reis, T. F. et al. A host defense peptide mimetic, brilacidin, potentiates caspofungin antifungal activity against human pathogenic fungi. *Nat. Commun.* **14**, 2052 (2023).
14. Lakshmaiah Narayana, J. et al. Two distinct amphipathic peptide antibiotics with systemic efficacy. *Proc. Natl. Acad. Sci. USA* **117**, 19446–19454 (2020).
15. Wang, M. et al. Development of bis-cyclic imidazolidine-4-one derivatives as potent antibacterial agents. *J. Med. Chem.* **63**, 15591–15602 (2020).
16. Wang, J. et al. Structural superiority of guanidinium-rich, four-armed copolypeptides: role of multiple peptide–membrane interactions in enhancing bacterial membrane perturbation and permeability. *ACS Appl. Mater. Interfaces* **12**, 18363–18374 (2020).
17. Xiong, M. et al. Bacteria-assisted activation of antimicrobial polypeptides by a random-coil to helix transition. *Angew. Chem. Int. Ed.* **56**, 10826–10829 (2017).
18. Jiang, W. et al. Peptide polymer displaying potent activity against clinically isolated multidrug resistant Pseudomonas aeruginosa in vitro and in vivo. *Biomater. Sci.* **8**, 739–745 (2020).
19. Gao, F., Shao, T., Yu, Y., Xiong, Y. & Yang, L. Surface-bound reactive oxygen species generating nanozymes for selective antibacterial action. *Nat. Commun.* **12**, 745 (2021).
20. Bai, H. et al. A supramolecular antibiotic switch for antibacterial regulation. *Angew. Chem. Int. Ed.* **54**, 13208–13213 (2015).
21. Li, X. et al. Supramolecular antibacterial materials for combatting antibiotic resistance. *Adv. Mater.* **31**, 1805092 (2019).
22. Tew, G. N., Scott, R. W., Klein, M. L. & DeGrado, W. F. De novo design of antimicrobial polymers, foldamers, and small molecules: from discovery to practical applications. *Acc. Chem. Res.* **43**, 30–39 (2010).
23. Liu, L. H. et al. Self-assembled cationic peptide nanoparticles as an efficient antimicrobial agent. *Nat. Nanotechnol.* **4**, 457–463 (2009).
24. Sun, J., Li, M., Lin, M., Zhang, B. & Chen, X. High antibacterial activity and selectivity of the versatile polysulfoniums that combat drug resistance. *Adv. Mater.* **33**, 2104402 (2021).
25. Choi, S. et al. De novo design and in vivo activity of conformationally restrained antimicrobial arylamide foldamers. *Proc. Natl. Acad. Sci. USA* **106**, 6968–6973 (2009).
26. Zhong, W. et al. Designer broad-spectrum polyimidazolium antibiotics. *Proc. Natl. Acad. Sci. USA* **117**, 31376–31385 (2020).
27. Lam, S. J. et al. Combating multidrug-resistant Gram-negative bacteria with structurally nanoengineered antimicrobial peptide polymers. *Nat. Microbiol.* **1**, 16162 (2016).
28. Xie, J. et al. Addressing MRSA infection and antibacterial resistance with peptoid polymers. *Nat. Commun.* **12**, 5898 (2021).
29. Chin, W. et al. A macromolecular approach to eradicate multidrug resistant bacterial infections while mitigating drug resistance onset. *Nat. Commun.* **9**, 14 (2018).
30. Zhang, H. et al. Switching from membrane disrupting to membrane crossing, an effective strategy in designing antibacterial polypeptide. *Sci. Adv.* **9**, eabn0771 (2023).
31. Schaefer, S. et al. A synthetic peptide mimic kills Candida albicans and synergistically prevents infection. *Nat. Commun.* **15**, 6818 (2024).
32. Wu, Y. et al. Host defense peptide mimicking antimicrobial amino acid polymers and beyond: Design, synthesis and biomedical applications. *Prog. Polym. Sci.* **141**, 101679 (2023).
33. Barman, S., Konai, M. M., Samaddar, S. & Haldar, J. Amino acid conjugated polymers: antibacterial agents effective against drug-resistant acinetobacter baumannii with no detectable resistance. *ACS Appl. Mater. Interfaces* **11**, 33559–33572 (2019).
34. Jiang, W. et al. Short guanidinium-functionalized poly(2-oxazoline)s displaying potent therapeutic efficacy on drug-resistant fungal infections. *Angew. Chem. Int. Ed.* **61**, e202200778 (2022).
35. Jiang, W., Wu, Y., Zhou, M., Song, G. & Liu, R. Advance and designing strategies in polymeric antifungal agents inspired by membrane-active peptides. *Chem. Eur. J.* **28**, e202202226 (2022).

36. Jiang, W. et al. Peptide-mimicking poly(2-oxazoline)s possessing potent antifungal activity and BBB penetrating property to treat invasive infections and meningitis. *J. Am. Chem. Soc.* **145**, 25753–25765 (2023).
37. Wu, Y. et al. An effective strategy to develop potent and selective antifungal agents from cell penetrating peptides in tackling drug-resistant invasive fungal infections. *J. Med. Chem.* **65**, 7296–7311 (2022).
38. Neuwelt, E. A. Mechanisms of disease: the blood-brain barrier. *Neurosurgery* **54**, 131–142 (2004).
39. Gabathuler, R. Approaches to transport therapeutic drugs across the blood–brain barrier to treat brain diseases. *Neurobiol. Dis.* **37**, 48–57 (2010).
40. Kang, T., Gao, X. & Chen, J. Harnessing the capacity of cell-penetrating peptides for drug delivery to the central nervous system. *Curr. Pharm. Biotechnol.* **15**, 220–230 (2014).
41. Rizzuti, M., Nizzardo, M., Zanetta, C., Ramirez, A. & Corti, S. Therapeutic applications of the cell-penetrating HIV-1 Tat peptide. *Drug Discov. Today* **20**, 76–85 (2015).
42. Terstappen, G. C., Meyer, A. H., Bell, R. D. & Zhang, W. Strategies for delivering therapeutics across the blood–brain barrier. *Nat. Rev. Drug Discov.* **20**, 362–383 (2021).
43. Zhou, Q. et al. Fluoroamphiphilic polymers exterminate multidrug-resistant Gram-negative ESKAPE pathogens while attenuating drug resistance. *Sci. Adv.* **10**, eadp6604 (2024).
44. Li, J. et al. Biguanide-derived polymeric nanoparticles kill MRSA biofilm and suppress infection in vivo. *ACS Appl. Mater. Interfaces* **12**, 21231–21241 (2020).
45. Rahn, H. P. et al. Biguanide-vancomycin conjugates are effective broad-spectrum antibiotics against actively growing and biofilm-associated gram-positive and gram-negative ESKAPE pathogens and mycobacteria. *J. Am. Chem. Soc.* **146**, 22541–22552 (2024).
46. Hervé, F., Ghinea, N. & Scherrmann, J.-M. CNS delivery via adsorptive transcytosis. *AAPS J.* **10**, 455–472 (2008).
47. Banks, W. A. From blood–brain barrier to blood–brain interface: new opportunities for CNS drug delivery. *Nat. Rev. Drug Discov.* **15**, 275–292 (2016).
48. Krumm, C. et al. Antimicrobial poly(2-methyloxazoline)s with bioswitchable activity through satellite group modification. *Angew. Chem. Int. Ed.* **53**, 3830–3834 (2014).
49. Hoogenboom, R. Poly(2-oxazoline)s: a polymer class with numerous potential applications. *Angew. Chem. Int. Ed.* **48**, 7978–7994 (2009).
50. Zhou, M. et al. Poly(2-Oxazoline)-based functional peptide mimics: eradicating MRSA Infections and persisters while alleviating antimicrobial resistance. *Angew. Chem. Int. Ed.* **59**, 6412–6419 (2020).
51. Zhou, M. et al. A dual-targeting antifungal is effective against multidrug-resistant human fungal pathogens. *Nat. Microbiol.* **9**, 1325–1339 (2024).
52. Bernatowicz, M. S., Wu, Y. L. & Matsueda, G. R. 1-H-pyrazole-1-carboxamidine hydrochloride: an attractive reagent for guanylation of amines and its application to peptide synthesis. *J. Org. Chem.* **57**, 2497–2502 (1992).
53. Deo, S., Turton, K. L., Kainth, T., Kumar, A. & Wieden, H.-J. Strategies for improving antimicrobial peptide production. *Biotechnol. Adv.* **59**, 107968 (2022).
54. Martin, J. K. et al. A dual-mechanism antibiotic kills gram-negative bacteria and avoids drug resistance. *Cell* **181**, 1518–1532.e1514 (2020).
55. Ciofu, O., Moser, C., Jensen, P. Ø. & Høiby, N. Tolerance and resistance of microbial biofilms. *Nat. Rev. Microbiol.* **20**, 621–635 (2022).
56. Feng, J. et al. A synthetic antibiotic class with a deeply-optimized design for overcoming bacterial resistance. *Nat. Commun.* **15**, 6040 (2024).
57. Weng, Z. et al. Antimicrobial activities of lavandulylated flavonoids in Sophora flavences against methicillin-resistant Staphylococcus aureus via membrane disruption. *J. Adv. Res.* **57**, 197–212 (2024).
58. Privalsky, T. M. et al. Prospects for antibacterial discovery and development. *J. Am. Chem. Soc.* **143**, 21127–21142 (2021).
59. De Gaetano, G. V., Lentini, G., Famà, A., Coppolino, F. & Beninati, C. Antimicrobial resistance: two-component regulatory systems and multidrug efflux pumps. *Antibiotics* **12**, 965 (2023).
60. Le Masters, T. et al. Comparative transcriptomic analysis of Staphylococcus aureus associated with periprosthetic joint infection under in vivo and in vitro conditions. *J. Mol. Diagn.* **23**, 986–999 (2021).
61. Zhu, H., Gong, L., Wang, R. & Shao, Z. The effects and toxicity of different pyrene concentrations on Escherichia coli using transcriptomic analysis. *Microorganisms* **12**, 326 (2024).
62. Wei, X., Hu, Y., Sun, C. & Wu, S. Characterization of a novel antimicrobial peptide bacipeptin against foodborne pathogens. *J. Agric. Food Chem.* **72**, 5283–5292 (2024).
63. Ji, Y., Sun, C. & Wu, S. Transcriptomic and biochemical analysis of the antimicrobial mechanism of lipopeptide Iturin W against Staphylococcus aureus. *Int. J. Mol. Sci.* **25**, 9949 (2024).
64. Tang, Y. et al. Overcoming the reticuloendothelial system barrier to drug delivery with a "Don't-Eat-Us" strategy. *ACS Nano* **13**, 13015–13026 (2019).
65. Watanabe, K. et al. In vivoassessment of the permeability of the blood-brain barrier and blood-retinal barrier to fluorescent indoline derivatives in zebrafish. *BMC Neurosci.* **13**, 101 (2012).
66. Xu, Z. et al. Converting organosulfur compounds to inorganic polysulfides against resistant bacterial infections. *Nat. Commun.* **9**, 3713 (2018).
67. Lu, M. et al. Bacteria-specific phototoxic reactions triggered by blue light and phytochemical carvacrol. *Sci. Transl. Med.* **13**, eaba3571 (2021).
68. Yarlagadda, V., Sarkar, P., Samaddar, S. & Haldar, J. A vancomycin derivative with a pyrophosphate-binding group: A strategy to combat vancomycin-resistant bacteria. *Angew. Chem., Int. Ed.* **55**, 7836–7840 (2016).
69. Nagarajan, D. et al. Ω76: A designed antimicrobial peptide to combat carbapenem- and tigecycline-resistant Acinetobacter baumannii. *Sci. Adv.* **5**, eaax1946 (2019).
70. Wei, X. et al. Supercharged precision killers: genetically engineered biomimetic drugs of screened metalloantibiotics against Acinetobacter baumanni. *Sci. Adv.* **10**, eadk6331 (2024).

Acknowledgements

This study was supported by the National Key Research and Development Program of China (No. 2024YFC2418700 (R.L.)), the Postdoctoral Fellowship Program of CPSF (GZB20240806 (W.J.)), Non-profit Central Research Institute Fund of Chinese Academy of Medical Sciences (2024-JKCS-07 (Y.W.)), the National Natural Science Foundation of China (No. T2325010 (R.L.), 52203162 (Y.W.), 22305082 (M.Z.)), the Basic Research Pilot Program of Suzhou (SSD2025009 (W.J.)), Shanghai "Science and Technology Innovation Action Plan" Computational Biology Program (24JS2830400 (R.L.)), Shanghai Frontiers Science Center of Optogenetic Techniques for Cell Metabolism (Shanghai Municipal Education Commission), Open Research Fund of State Key Laboratory of Polymer Physics and Chemistry (Changchun Institute of Applied Chemistry, Chinese Academy of Sciences), the Open Project of Engineering Research Center of Dairy Quality and Safety Control Technology (Ministry of Education, R202201 (R.L.)), the China Postdoctoral Science Foundation (2024M763493 (W.J.), 2025T180971 (W.J.)). We thank the Analysis and Testing Center of the East China University of Science and Technology for their help in the characterization. We thank the Analysis and Testing Center of the School of Chemical Engineering, East China

University of Science and Technology for the support. We thank the staff members of the Integrated Laser Microscopy System at the National Facility for Protein Science in Shanghai (NFPS), Zhangjiang Lab, China, and Hubei BIOSSCI Biotechnology Co., Ltd for providing technical support and assistance in data.

Author contributions

R.L. directed and oversaw the whole project. W.J., R.L. and Y.W. conceived the idea, designed the experiments, and wrote the manuscript together. W.J. performed most of the experiments. M.Z. contributed to the synthesis of the monomers and polymers, and the fluorescent dye. K.C. contributed to computational study. X.X. contributed to RNA-seq study. J.S. contributed to ITC test. H.Z. and J.X. operated the SEM test and participated in peritonitis model. S.C. contributed to the in vitro transwell study and participated in meningitis model. M.C., Z.C. and L.L. participated in vivo animal models. All authors gave suggestions to prepare and improve the manuscript.

Competing interests

R.L. and W.J. are co-inventors on a patent application covering the function of polymers presented in this report. The remaining authors declare no competing interests.

Additional information

Supplementary information The online version contains supplementary material available at https://doi.org/10.1038/s41467-025-67044-5.

Correspondence and requests for materials should be addressed to Yueming Wu or Runhui Liu.

Peer review information *Nature Communications* thanks Francesco Maione, who co-reviewed with Anella Anella Saviano, Susu Zughaier and the other, anonymous, reviewer(s) for their contribution to the peer review of this work. A peer review file is available.